Society of Medical Education & Research

2022, Volume 2, Issue 1, Page No: 58-84
ISSN: 3108-4826

Journal of Medical Sciences and Interdisciplinary Research

Regulation of GLUT1 Deubiquitination by UBE2S–USP10 Reprograms Metabolism and Immunity in Endometriosis

Laura Beatrice Conti[1]*, Marco Antonio De Santis[1], Chiara Lucia Bianchi[1]

[1]Department of Management, Catholic University of the Sacred Heart, Milan, Italy.

***E-mail** ✉ l.conti.ucsc@outlook.com

Abstract

Endometriosis (EM) represents a persistent inflammatory condition marked by the presence of endometrium-like tissue outside its normal location and associated fibrotic changes. Alterations in metabolism, notably heightened glycolytic processes, along with disruptions in the immune milieu, constitute prominent aspects of EM advancement. Nonetheless, the precise molecular pathways involved are still inadequately clarified. The present investigation employed a combination of transcriptome profiling, immunoprecipitation-mass spectrometry (IP-MS), co-immunoprecipitation, and ubiquitination experiments to thoroughly explore the function of Ubiquitin-Conjugating Enzyme E2S (UBE2S) in controlling glucose metabolism and immune regulation within EM. Cellular assays in vitro, along with murine models, were utilized to confirm its influence on glycolytic pathways, macrophage polarization states, and fibrotic development. Expression of UBE2S was markedly elevated in stromal cells from ectopic endometriotic sites. Through IP-MS, GLUT1 and USP10 emerged as principal partners interacting with UBE2S. Detailed mechanistic examinations demonstrated that UBE2S facilitates K48-linked deubiquitination of GLUT1 via USP10, thereby maintaining GLUT1 protein stability and augmenting glycolytic flux. Such metabolic shifts result in increased lactate buildup, which in turn triggers M2-type macrophage polarization and release of TGF-β1, consequently driving the conversion of fibroblasts to myofibroblasts and hastening lesion fibrosis. Administration of the UBE2S inhibitor cephalomannine notably reduced GLUT1 levels, curtailed glycolysis, impeded M2 polarization, and mitigated fibrosis in ectopic sites. The research elucidates the pathway whereby the UBE2S–USP10–GLUT1 axis modulates the immune surroundings and advances fibrosis in EM via alterations in metabolism. These observations yield fresh perspectives on EM pathophysiology and establish a rationale for pursuing UBE2S as a target in treatment approaches.

Keywords: Endometriosis, UBE2S, GLUT1, USP10, Glycolysis, M2 macrophage polarization

Introduction

Endometriosis (EM) constitutes a longstanding gynecological condition defined by the development of endometrium-resembling tissue beyond the uterus, resulting in ongoing inflammation, fibrotic alterations, and clinical issues like pelvic discomfort and subfertility [1, 2]. Despite extensive prior research into its origins, the core molecular processes continue to be elusive. Mounting data point to critical involvement of metabolic shifts and immune imbalances in EM evolution, chiefly through modified glucose handling and impaired immune cell activity [3, 4].

Lesions in endometriosis (EM) show a metabolic pattern dominated by glycolysis, where lactate arising from irregular glucose processing acts as an essential link connecting ectopic tissues to immune components. Elevated lactate fosters M2 macrophage polarization, modifying the immune context and facilitating immune escape [5]. These M2 macrophages additionally drive fibrosis via stimulation of fibroblast transformation into myofibroblasts [4, 5]. Accordingly, immune regulation mediated by lactate potentially bridges glucose

Access this article online https://smerpub.com/

Received: 12 November 2021; **Accepted:** 08 February 2022

How to cite this article: Conti LB, Santis MAD, Bianchi CL. Regulation of GLUT1 Deubiquitination by UBE2S–USP10 Reprograms Metabolism and Immunity in Endometriosis. J Med Sci Interdiscip Res. 2022;2(1):58-84. https://doi.org/10.51847/DMofvX2jn9

metabolism to fibrotic advancement in EM. Inhibiting key metabolic components may yield innovative options for diagnosis and therapy, although the exact control processes require further definition.

Ubiquitination serves as an important post-translational alteration that governs protein stability and activity, exerting significant influence on cell metabolism and immune equilibrium in diverse disorders [6, 7]. UBE2S stands out as a distinctive E2 ubiquitin-conjugating enzyme featuring E3-dependent as well as independent ligase capabilities [8], and it has been linked to protein breakdown and cancer advancement [9, 10]. Yet, its involvement in endometriosis remains unclarified. Via IP/MS analysis, an association was uncovered between UBE2S and the glucose transporter GLUT1. This vital glycolysis controller supports glucose entry and boosts lactate production [11]. Beyond metabolism, lactate functions as a pivotal immunomodulatory agent capable of promoting M2 macrophage polarization [12]. While UBE2S and GLUT1 are each connected separately to ubiquitination processes and metabolic control, their interactive role in endometriosis is undetermined. The current work seeks to determine if UBE2S influences GLUT1 ubiquitination and protein stability, thus affecting the metabolic and immunological shifts observed in endometriosis.

In the present investigation, we examined the function of UBE2S in endometriosis (EM) and put forward the concept that UBE2S increases GLUT1 protein stability by facilitating its deubiquitination via Ubiquitin-Specific Peptidase 10 (USP10). This mechanism supports alterations in cellular metabolism, shifts in macrophage phenotypes, and fibrotic development in lesions. Through detailed exploration of this axis both in cellular systems and animal models, our objective was to reveal a novel understanding of the metabolism-immune interaction in EM and highlight possible intervention points for treatment.

Materials and Methods

Patients and samples

Samples of endometrial tissue were obtained from 20 patients diagnosed with ovarian endometriotic cysts and from individuals with other non-endometriotic conditions (such as leiomyomas of the uterus and cervical intraepithelial lesions) who received total hysterectomy at the First Affiliated Hospital of Harbin Medical University. The collection comprised 20 specimens of ectopic endometrium (EC), 20 of eutopic endometrium (Eu), and 20 of normal endometrium (NM) from patients without endometriosis. From the 20 clinical samples in each category, 5 were designated for immunohistochemistry, while the other 15 were processed for primary stromal cell isolation. After strict double-marker phenotyping ($Vimentin^+/Cytokeratin^-$), only cultures achieving >95% purity across passages 2–3 were employed in further procedures, encompassing RNA sequencing, nucleic acid/protein isolation, assays for cell growth and movement, and metabolic evaluations. Inclusion requirements included: age between ≥18 and ≤50 years, premenopausal status with regular cycles (28 ± 7 days), absence of oral contraceptives, injectable or implantable contraception, intrauterine devices, or hormone therapy for at least three months before collection. Exclusion factors were: age outside 18–50 years, postmenopausal condition, lack of postoperative pathological confirmation of EM in the study group, or any endometrial abnormalities in controls. All procedures received approval from the Ethics Committee of the First Affiliated Hospital of Harbin Medical University, with written informed consent provided by every participant.

Isolation and culture of endometrial stromal cells

Stromal cells from ectopic endometrium (EESCs), eutopic endometrium (EuSCs), and normal endometrium (NESCs) were separated via enzymatic treatment using type IV collagenase (1 mg/mL, Biosharp) at 37 °C. Following filtration and centrifugation steps, cells were placed in DMEM/F12 medium (GIBCO, NY, USA) supplemented with 10% FBS and maintained at 37 °C in an atmosphere containing 5% CO_2.

RNA sequencing (RNA-seq)

Total RNA isolation was carried out with Trizol reagent (Invitrogen, CA, USA). Assessment of RNA quality and completeness involved NanoDrop 2000 (Thermo Fisher, USA) and Bioanalyzer 2100 (Agilent, USA), alongside verification of integrity on 1.5% agarose gels. mRNA enrichment utilized Poly-T magnetic beads, and library construction employed the VAHTS Universal V6 RNA-seq Library Kit for MGI (Vazyme, China). Library validation occurred via Qubit 3.0 (Thermo Fisher, USA) and Bioanalyzer 2100, with subsequent sequencing performed on the MGI-SEQ 2000 system (Frasergen, Wuhan, China). Initial reads underwent filtering using SOAPnuke (v2.1.0) to eliminate adapters, poor-quality

sequences, and those with excessive unknown bases. Processed reads were mapped to the reference genome through HISAT2 (v2.1.0) and Bowtie2 (v2.3.5). Expression levels were calculated with RSEM (v1.3.1) and expressed as FPKM. Identification of differentially expressed genes relied on DESeq2 (v1.22.2), applying criteria of |log2FC| >1 and false discovery rate (FDR) < 0.05 for significance.

Gene ontology (GO) and gene set enrichment analysis (GSEA)

Enrichment analysis of GO terms for differentially expressed genes was conducted via the enrichGO tool in the R package clusterProfiler (v3.6.3). Terms achieving p value ≤ 0.05 were deemed significantly enriched. Graphical representation of GO findings was generated with ggplot2 (v3.5.1) from R. For GSEA, a ranked list of all detected genes served as input, evaluated against Hallmark gene sets from the Molecular Signatures Database (MSigDB). Analysis used the GSEA tool within clusterProfiler (v3.6.3), with settings: minimum gene set size = 0, maximum = 20,000, no p value cutoff, Benjamini–Hochberg adjustment for multiple testing, and 1,000 permutations. Gene sets showing normalized enrichment score (NES) > 1 (or < −1), p value < 0.05, and FDR < 0.25 were classified as significantly enriched. Plots of GSEA outcomes were created using the gseaNb function in the R package GseaVis (v0.0.5).

STRING protein–protein interaction (PPI) network analysis

Interactions among proteins encoded by differentially expressed genes were explored through the STRING database (https://string-db.org/). The constructed network was displayed and examined further in Cytoscape (v3.9.1) to detect central hub genes and important regulatory clusters.

Macrophage polarization

THP-1 cells (ScienCell) were induced to become M0 macrophages by exposure to 100 ng/ml phorbol 12-myristate 13-acetate (PMA; Sigma-Aldrich, St. Louis, MO, USA) for 24 h. Upon microscopic confirmation of adhesion and extended morphology, the PMA-containing medium was replaced with standard complete medium to halt induction. A transwell system featuring 0.4 μm pores (Corning, NY, USA) was applied. Differentially treated EESCs were placed in the upper insert, whereas M0 macrophages occupied the lower compartment. Following 48 h of co-incubation, lower-chamber cells were collected for evaluation of M2 markers (CD163, CD206, ARG-1).

Mass spectrometry analysis

Protein bands were removed from Coomassie Brilliant Blue–stained gels, reduced using DTT, alkylated with iodoacetamide, and subjected to overnight tryptic digestion. Peptides were recovered in acetonitrile, purified on ZipTip C18 columns, and examined by LC–MS/MS using a nanoLC-Q Exactive instrument (Thermo Scientific, USA). Raw spectra were queried against the UniProt human proteome database (2022 release) via the SEQUEST HT search engine in Proteome Discoverer (v1.4). Parameters included: full trypsin specificity allowing up to two missed cleavages, 10 ppm precursor tolerance, 0.02 Da fragment tolerance, fixed carbamidomethylation on cysteine, and variable methionine oxidation. Identifications were refined with Percolator to achieve a 1% FDR for high-confidence peptides.

Creation of cell lines deficient in USP10 or UBE2S

Lines devoid of USP10 and UBE2S were developed via the CRISPR/Cas9 methodology. To produce cells without USP10, guide RNAs aimed at USP10 were incorporated into the PX459 plasmid and delivered into HEK293T cells employing Lipofectamine 3000. Following a 24 h period, selection involved puromycin (2 μg/mL) over 48 h. Isolated single clones underwent expansion and verification via PCR combined with Western blot procedures. An analogous strategy was applied for knocking out UBE2S in HEK293T as well as EESCs. Guide RNAs designed for UBE2S were placed into PX459, with subsequent delivery and puromycin-based screening. Confirmation of effective gene disruption in chosen clones relied on PCR and Western blot techniques.

Introduction of plasmids and development of stable lines

Plasmids utilized recombinantly in this work comprised pCAGGS-UBE2S (bearing Flag, HA, and Myc tags), pCMV-Flag-UBE2S ΔN, pCMV-Flag-UBE2S ΔC, and pCMV-Flag-UBE2S ΔCore, supplied courtesy of Professor Changjiang Weng from the Harbin Veterinary Research Institute. Custom short hairpin RNAs directed against UBE2S and GLUT1 were produced synthetically, accompanied by nonspecific control sequences. Annealing of these synthetic pieces was followed by

restriction using BamH I and EcoR I, then insertion into pLVX-shRNA1 (Clontech, Palo Alto, USA). Delivery into cells occurred through Lipofectamine 3000. Production of lentiviruses required joint introduction into HEK293T of desired constructs together with auxiliary vectors psPAX2 and pMD2.G.

CCK8 assay for assessing cell growth

Seeding occurred at 2000 cells per well across 96-well formats, with incubation spanning 24, 48, and 72 h. Addition of 10 µL CCK-8 reagent (Meilunbio, Dalian, China) preceded measurement of absorbance values at 450 nm.

EdU-based evaluation of proliferative activity

Placement involved 1 × 10^5 cells per well in 12-well setups, followed by 4 h exposure to EdU (Beyotime Biotechnology, Shanghai, China), fixation, and dye application. Resulting fluorescent patterns were documented via microscopy.

Scratch wound assay

Cells after treatment were transferred to six-well formats. At near 90% density, a linear injury was inflicted using a tip. Removal of detached material via PBS wash preceded initial imaging at 0 h. Further cultivation for 24 h allowed repeat photography.

Transwell system for assessing cell movement

Suspensions at 2.5 × 10^5 cells/mL occupied upper compartments of 24-well transwell units (Corning, NY, USA) featuring 8 µm membranes, under conditions lacking serum. Lower sections held DMEM enriched with 20% FBS. Incubation at 37 °C lasted 24 h, after which fixation was employed 4% paraformaldehyde (15 min), PBS rinses, crystal violet application (20 min), additional washes, and imaging for quantitation.

Assays for glucose consumption and levels of lactate/pyruvate

Cells following plasmid introduction were moved to six-well dishes and allowed 12–16 h growth. Collection enabled determination of glucose, lactate, and pyruvate amounts via specialized kits (mlbio, Shanghai, China).

Immunohistochemical procedures (IHC)

H&E involved xylene-based deparaffinization of 5 µm sections, hematoxylin-eosin sequence, and bright-field viewing. IHC on 4 µm slices included deparaffinization, hydration steps, and 15 min exposure to 3% H2O2 for peroxidase blocking. Retrieval used citrate (pH 9.0), with 30 min goat serum block. Overnight 4 °C exposure to primaries—UBE2S (1:200, Proteintech) or GLUT1 (1:200, Proteintech)—preceded 1 h secondary (HRP-linked), DAB revelation, and viewing. ImageJ (NIH, Bethesda, MD, USA) quantified intensity and positive regions. Per specimen, five unrelated fields at 20× yielded averages. Analyses maintained blinding.

Co-Immunoprecipitation Protocol (Co-IP)

Harvested cells underwent disruption in buffer (50 mM Tris, pH 7.6, 0.5 mM EDTA, 0.1% NP40, 0.5 mM PMSF). Centrifugation allowed BCA-based quantitation (Beyotime, Shanghai, China). A fifth portion acted as input; the rest received target antibody and agarose for an overnight 4 °C rotation. Buffer washes are preceded by 10 min boil, then Western blot or spectrometric examination.

GST-based affinity isolation

Expression of pGEX-4T-1-UBE2S occurred in E. coli BL21 (DE3) via 1 mM IPTG induction. Harvested material received inhibitor-supplemented buffer, sonication, and spin (12,000 × g, 20 min, 4 °C). Cleared fraction with GST-UBE2S bound glutathione beads overnight at 4 °C. His-USP10 (from pET-24a(+)-USP10) joined immobilized fusion for 2 h at 4 °C. Multiple washes (4–5) allowed SDS buffer elution/boil, electrophoretic separation, and His-directed immunoblot.

Isolation of RNA, cDNA preparation, and quantitative PCR

Cell-derived total RNA came via Trizol (Invitrogen, CA, USA), with NanoDrop quantitation (Thermo Fisher Scientific, MA, USA). Conversion to cDNA used a dedicated kit (Seven, Beijing, China). Amplification relied on S6 Universal SYBR qPCR Mix (Enzy Artisan, Shanghai, China).

Molecular docking evaluation

To investigate the interaction preference of cephalomannine (CPM) for UBE2S and detect possible nonspecific bindings, computational docking was carried out employing AutoDock Vina (v1.2.5). Protein coordinates were retrieved from the UniProt repository (www.uniprot.org) and prepared via ADFRsuite-1.0. Target files in PDBQT format retained native ionization and charge distributions. The small-molecule structure of CPM was similarly handled with ADFRsuite-1.0 to

produce its PDBQT representation. Simulations utilized 32 parallel processing cores, a grid interval of 0.375, with remaining settings unchanged. Interaction strengths were estimated from Vina scores (ΔG), wherein more negative figures signify greater anticipated affinity.

In vivo studies

For assessing UBE2S contribution to endometriosis within a living system, a homologous graft model was adopted. Mice lacking UBE2S (UBE2S–/–) on the C57BL/6J strain were produced through targeted recombination (Biocytogen, Beijing, China. Female animals, either wild-type C57BL/6J or UBE2S–/–, aged 6–8 weeks, were given intraperitoneal estrogen (1 μg/mL) on days 1, 4, and 7. On day eight, donors were humanely sacrificed under sedation, the uterine horn endometrium was harvested, and it was resuspended in PBS. Aliquots of 0.6 mL suspension were administered intraperitoneally into pairs of immunocompetent C57BL/6J recipients. Weekly estrogen continued thereafter. Ectopic growths were recovered after four weeks. In therapeutic trials, animals were allocated randomly to weekly intraperitoneal CPM (10 mg/kg) or vehicle starting seven days post-implantation (n = 6 per cohort). Lesions were excised following four weeks of administration for examination. Every procedure involving animals gained approval from the Animal Ethics Committee of the First Affiliated Hospital of Harbin Medical University and adhered to relevant regulatory standards.

Data interpretation

Analyses employed SPSS (version 20.0) alongside GraphPad Prism (version 8.0). Group comparisons utilized one-way ANOVA with subsequent Tukey adjustment. Results achieving $p < 0.05$ were deemed significant.

Results and Discussion

UBE2S emerges as the primary ubiquitin-proteasome component linked to EESCs

In pursuit of candidate markers for endometriosis, RNA sequencing was performed on three normal and three ectopic stromal cell samples. Per the filtration pipeline **(Figure 1a),** duplicate entries were eliminated, retaining dominant isoforms for multi-transcript genes**.** Applying cutoffs of |log2FC| >1 and FDR < 0.001 yielded 4,404 genes showing altered expression. Enrichment assessments via GO and GSEA highlighted critical activities and routes in the condition. GO terms for these genes prominently featured processes like “positive control of proteolysis”, “control of protein ubiquitination”, “enhanced ubiquitin-reliant protein breakdown”, and “proteolysis of membrane proteins”**.** Concurrent GSEA on ranked gene lists disclosed notable activation of sets including “Positive Control of Protein Metabolism”, “Activator Role in Ubiquitin Transfer”, and “Enhanced Proteolysis”**.** Such patterns indicate transcriptional perturbation of ubiquitin-driven degradation routes in endometriosis, potentially driving pathogenesis. A compiled set of 181 ubiquitin-proteasome pathway genes [13] was cross-referenced with the 4,404 altered genes, uncovering 28 differentially regulated members (8 elevated, 20 reduced). These informed a volcanic display **(Figure 1b)** marking the 28 candidates, plus a clustered heat map illustrating their profiles **(Figure 1c).** Immune infiltration estimates here derive from xCell computations via the IOBR R package [14]. Abundance scores for immune populations were correlated (Pearson) with levels of the 28 pathway genes. Stringent criteria (p-value < 0.0001, absolute correlation >0.9) isolated three top-associated genes, presented in a Venn layout **(Figure 1d).** Protein interaction mapping of the 28 candidates through STRING positioned UBE2S as the most connected node **(Figure 1e)**. Network centrality alone, however, does not prove disease relevance. Accordingly, UBE2S levels were confirmed in ectopic cells, followed by targeted assays to define its involvement in endometriosis biology.

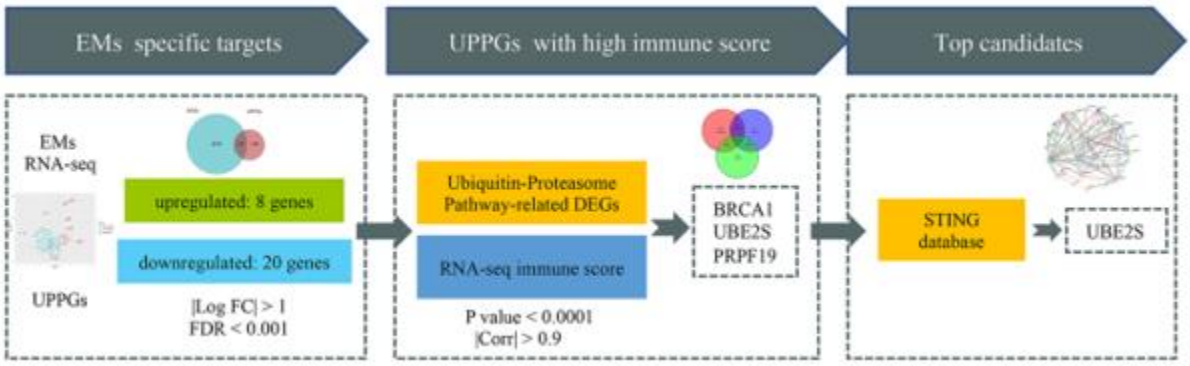
EMs specific targets
UPPGs with high immune score
Top candidates
EMs
RNA-seq
upregulated: 8 genes
downregulated: 20 genes
UPPGs
|Log FC| > 1
FDR < 0.001
Ubiquitin-Proteasome
Pathway-related DEGs
RNA-seq immune score
P value < 0.0001
|Corr| > 0.9
BRCA1
UBE2S
PRPF19
STING
database
UBE2S

a)

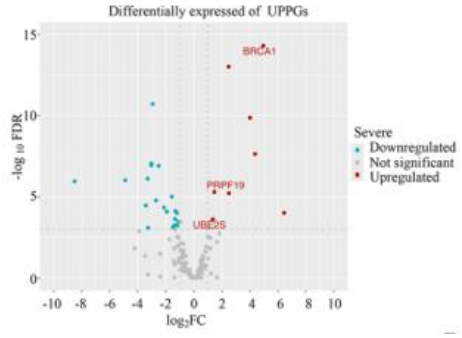
Differentially expressed of UPPGs
-log 10 FDR
log2FC
BRCA1
PRPF19
UBE2S
Severe
Downregulated
Not significant
Upregulated

b)

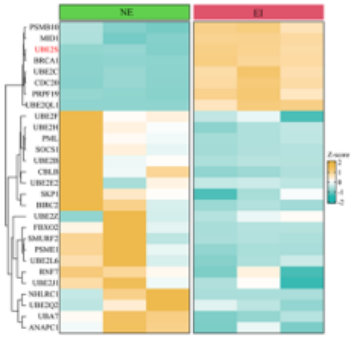
NE
EI

c)

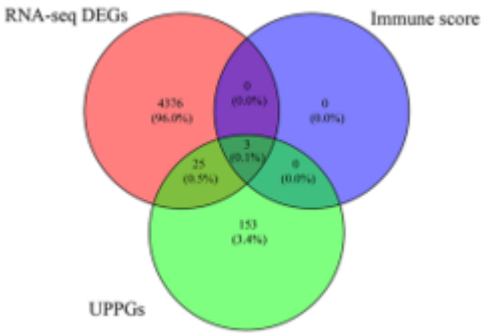
RNA-seq DEGs
Immune score
UPPGs
4336
(96.0%)
0
(0.0%)
0
(0.0%)
3
(0.1%)
25
(0.5%)
0
(0.0%)
153
(3.4%)

d)

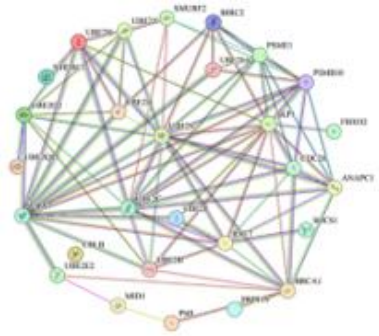

e)

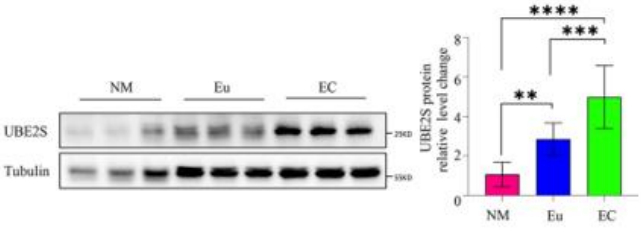
NM
Eu
EC
UBE2S
Tubulin
25KD
55KD
UBE2S protein
relative level change
****
***
**
NM
Eu
EC

f)

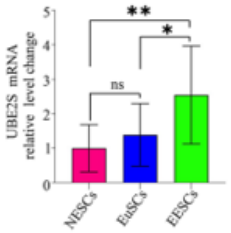
UBE2S mRNA
relative level change
**
*
ns
NESCs
EnSCs
EESCs

g)

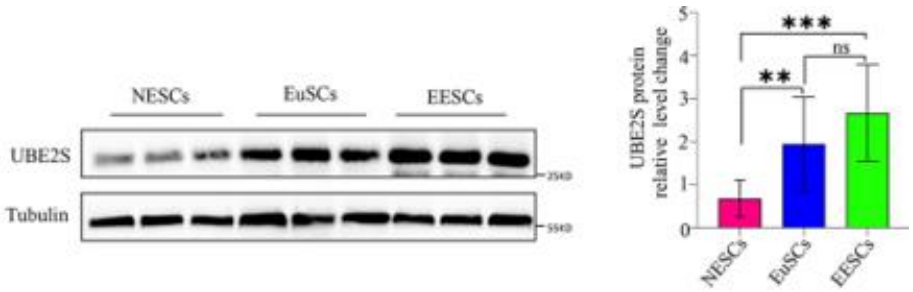

h)

Figure 1. Elevated levels of UBE2S in endometriosis relative to healthy endometrial tissue. (a) Schematic outlining the approach for pinpointing UBE2S as a preferentially involved gene within endometriosis transcriptome datasets. (b) Volcanic representation highlighting altered expression of ubiquitin-proteasome pathway components across compared cohorts. (c) Clustered heat map portraying expression variances of ubiquitin-proteasome pathway elements between cohorts. (d) Venn illustration showing intersections among endometriosis transcriptome findings, ubiquitin-proteasome pathway components, and immune-related profiles. (e) Protein interaction network derived from STRING for the 28 selected genes. (f) Immunoblot examination of UBE2S protein in normal (NM), eutopic (Eu), and ectopic (EC) endometrial samples. (g) Quantitative RT-PCR measurement of UBE2S transcript abundance in normal stromal cells (NESCs), eutopic stromal cells (EuSCs), and ectopic stromal cells (EESCs). (h) Immunoblot detection of UBE2S protein abundance in NESCs, EuSCs, and EESCs. * $p < 0.05$, ** $p < 0.01$, *** $p < 0.001$, **** $p < 0.0001$

For verification of UBE2S abundance in endometriosis, immunoblotting was conducted across 12 matched sets of ectopic (EC), eutopic (Eu), and normal (NM) endometrial specimens. Outcomes demonstrated markedly higher UBE2S protein content in ectopic samples versus normal counterparts **(Figure 1f).** Parallel assessments of transcript and protein in isolated stromal cells disclosed substantial increases of UBE2S both transcriptionally **(Figure 1g)** and translationally **(Figure 1h)** within ectopic stromal populations. Collectively, these observations point to overexpression of UBE2S in endometriotic lesions and derived cells.

UBE2S influences key cellular activities in EESCs

To delineate the functional contribution of UBE2S in ectopic stromal cells, lines with enforced expression or silenced UBE2S were established, and impacts on growth and motility were examined. Growth effects were initially probed via CCK-8 and EdU methodologies. Enforced UBE2S led to notable enhancement of cellular expansion (**Figures 2a and 2c**; $p < 0.05$), while suppression markedly reduced it (**Figures 2b and d**; $p < 0.01$). Motility was further interrogated through Transwell and wound closure tests. Elevated UBE2S substantially augmented migratory potential (**Figures 2e and 2g**; $p < 0.05$), whereas depletion curtailed it (**Figures 2f and 2h**; $p < 0.001$). Such cellular studies underscore that UBE2S drives both expansion and movement of ectopic stromal cells, implicating it centrally in endometriosis development.

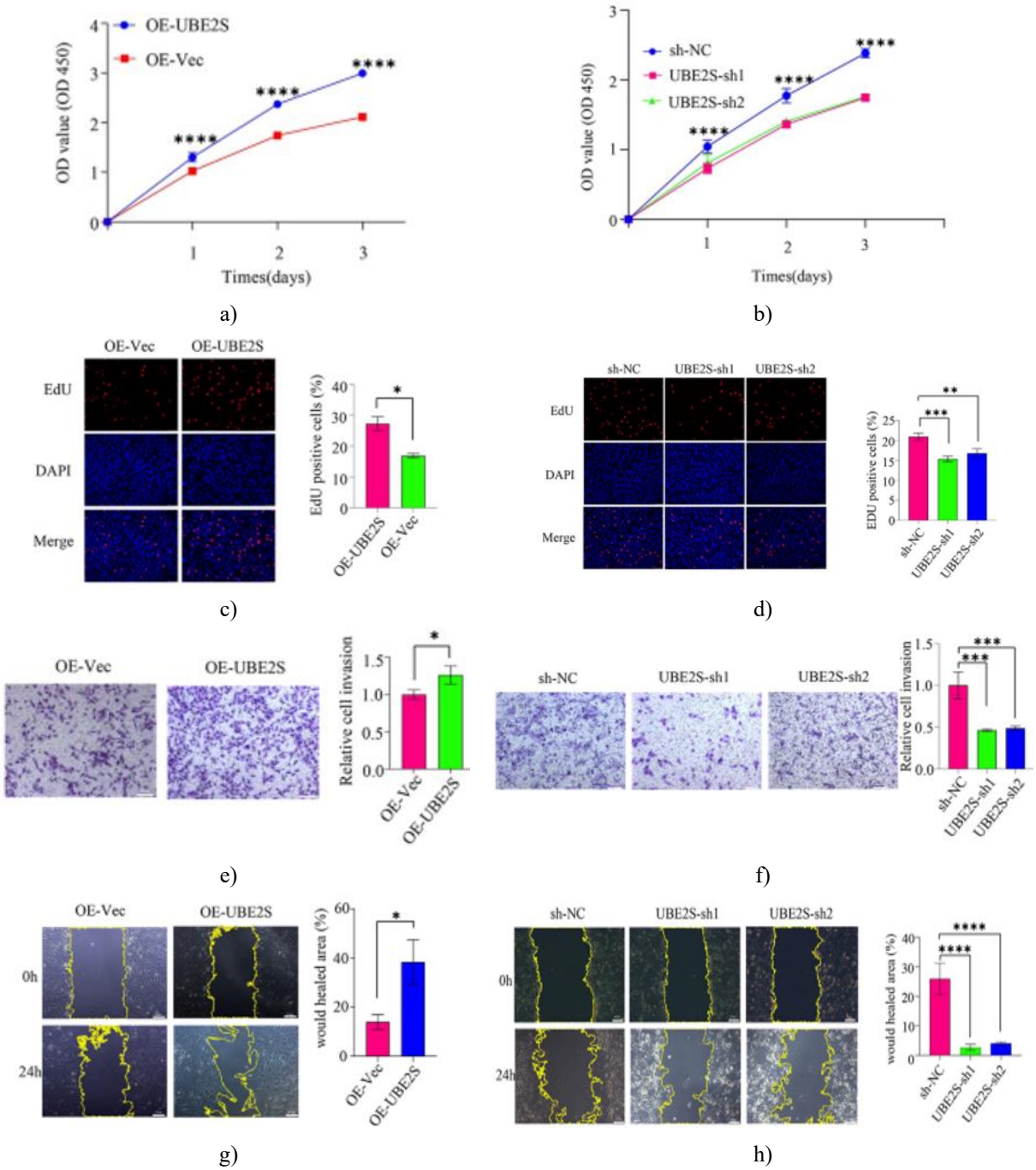

Figure 2. UBE2S enhances the growth and motility of ectopic stromal cells under culture conditions. (a-b) CCK-8 evaluation of proliferative rates in EESCs following UBE2S gain or loss. (c-d) EdU incorporation assay reflecting proliferative changes after UBE2S modulation. (e-f) Transwell quantification of migratory behavior post-UBE2S alteration. (g-h) Wound healing assessment of motility under UBE2S overexpression or reduction. * $p < 0.05$, ** $p < 0.01$, *** $p < 0.001$, **** $p < 0.0001$

UBE2S associates with GLUT1 in a complex and controls lactate production pathways

In pursuit of deeper mechanistic insights into UBE2S actions in endometriosis, Flag-tagged UBE2S was introduced into ectopic stromal cells, with an empty Flag

vector serving as a control. Immunoprecipitation uncovered a distinct band exclusive to the tagged group **(Figure 3a).** Targeted proteomic sequencing of this band via LC–MS/MS pinpointed GLUT1 as a candidate interactor. Endogenous confirmation employed monoclonal antibodies against each protein in cell lysates, verifying GLUT1 capture by UBE2S pull-down **(Figure 3b)** and reciprocal detection of UBE2S in GLUT1 isolates **(Figure 3c).** Additional validation involved dual delivery of Flag-GLUT1 and HA-UBE2S into 293T cells, with bead-based isolation revealing mutual co-enrichment**.** Domain mapping via truncated HA-UBE2S variants (ΔC, ΔN, ΔCore) in co-precipitation showed binding of GLUT1 to wild-type, ΔC, and ΔCore forms, but absence with ΔN**.** These data establish cellular complex formation between UBE2S and GLUT1, dependent critically on the N-terminal region of UBE2S.

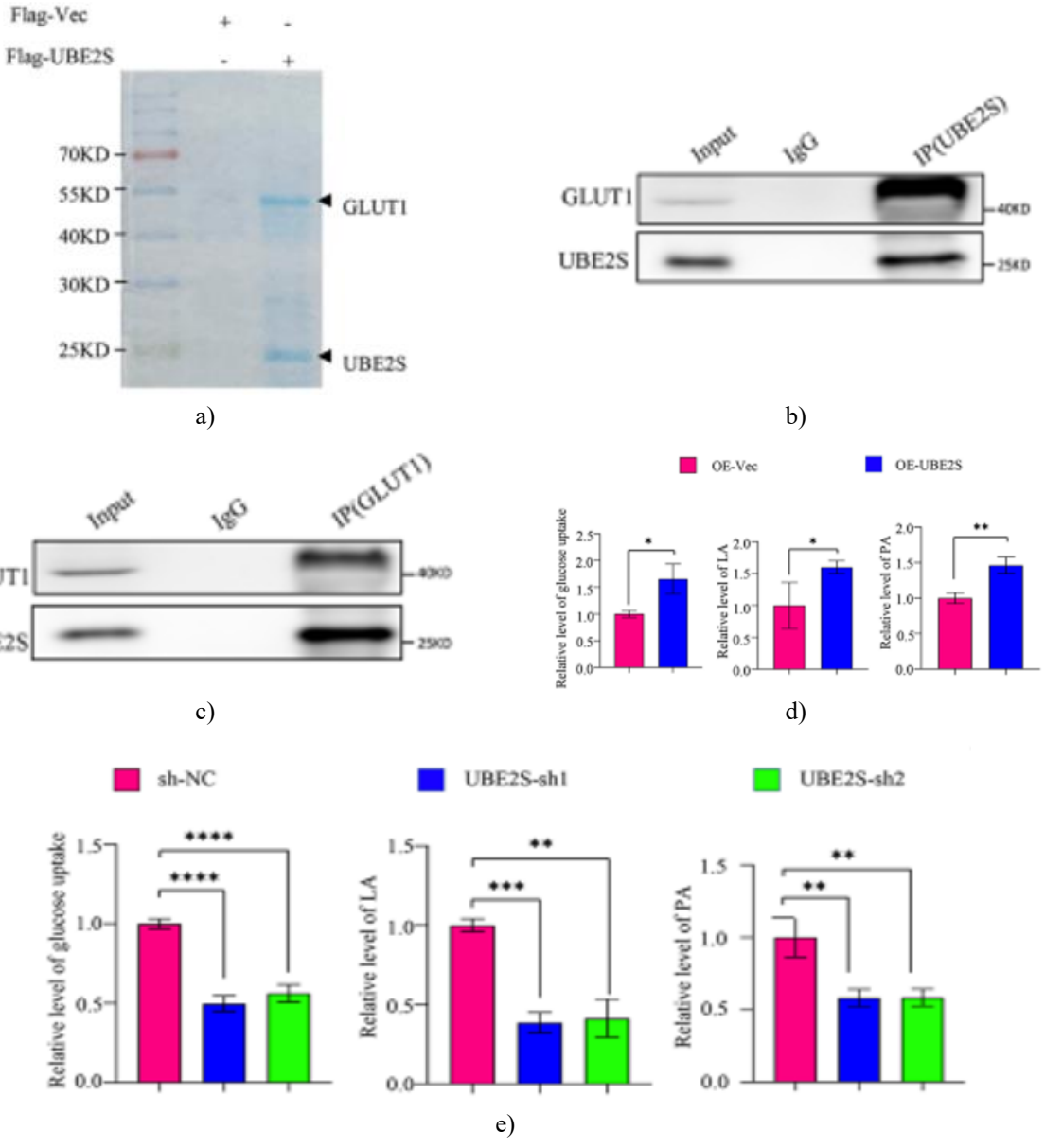

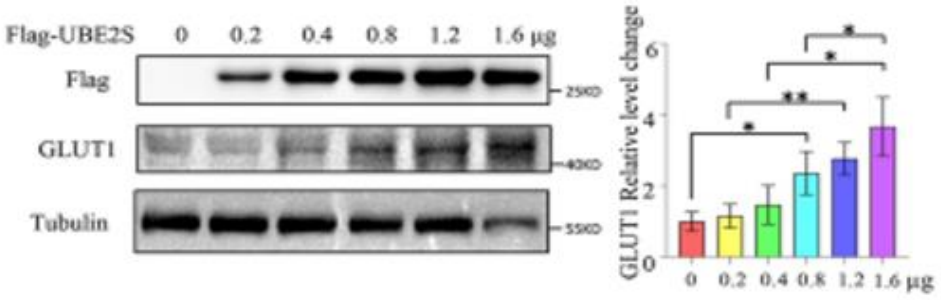
Flag-UBE2S 0 0.2 0.4 0.8 1.2 1.6 μg
Flag
GLUT1
Tubulin
25KD
40KD
55KD
GLUT1 Relative level change
0 0.2 0.4 0.8 1.2 1.6 μg

f)

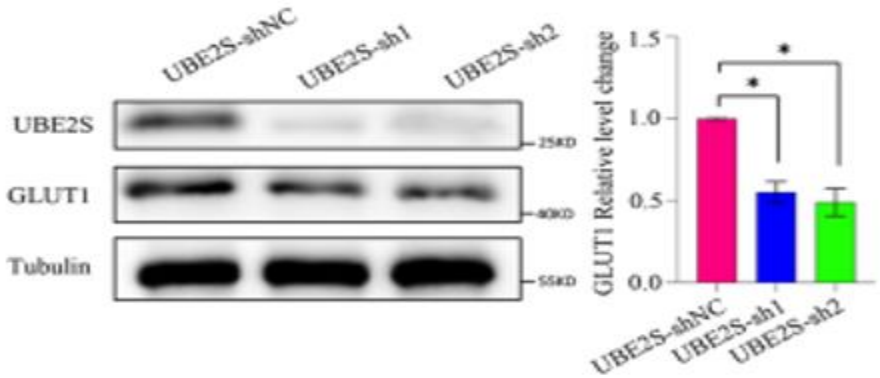
UBE2S-shNC
UBE2S-sh1
UBE2S-sh2
UBE2S
GLUT1
Tubulin
25KD
40KD
55KD
GLUT1 Relative level change
UBE2S-shNC
UBE2S-sh1
UBE2S-sh2

g)

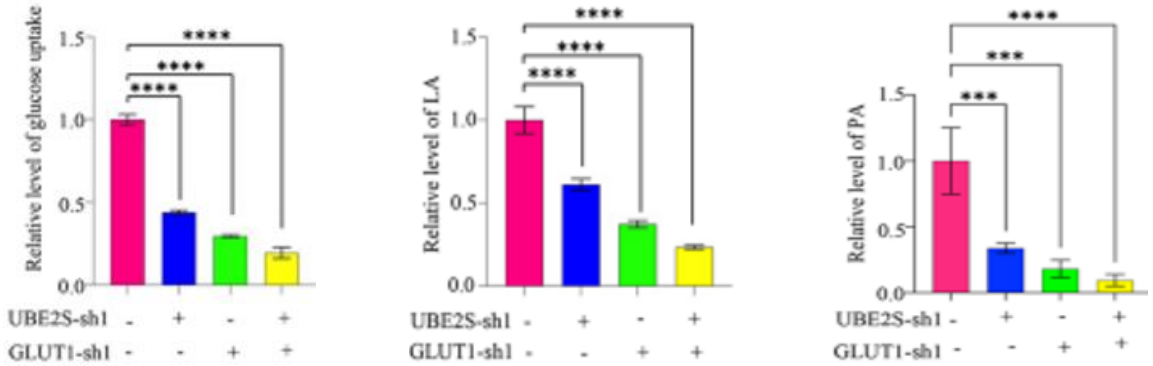
Relative level of glucose uptake
UBE2S-sh1
GLUT1-sh1
Relative level of LA
Relative level of PA

h) i) j)

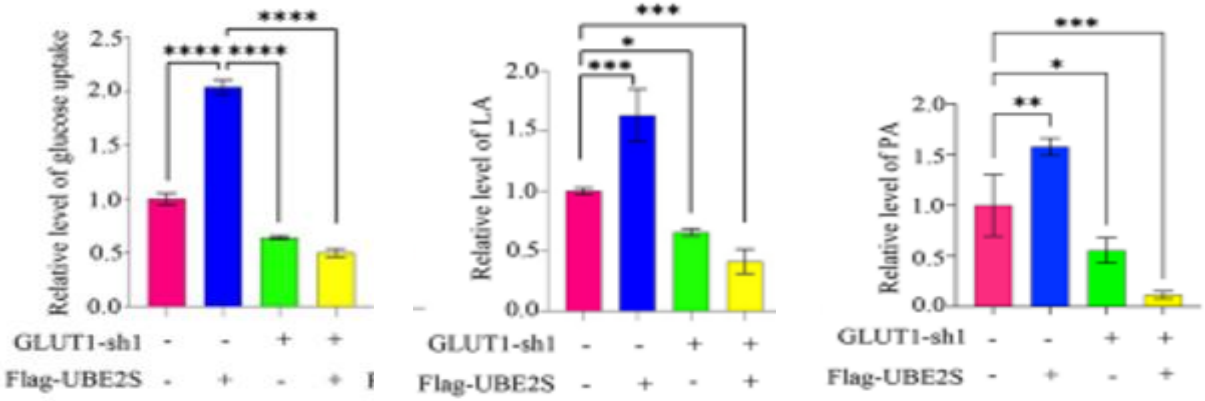
Relative level of glucose uptake
GLUT1-sh1
Flag-UBE2S
Relative level of LA
Relative level of PA

k) l) m)

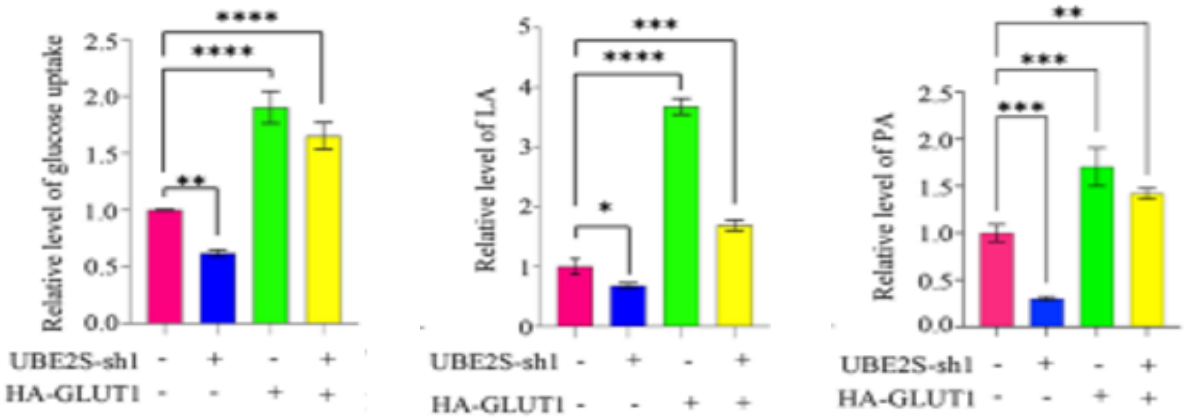

n) o) p)

Figure 3. UBE2S associates with GLUT1 to drive glycolytic activity in ectopic stromal cells. (a) Proteomic identification of GLUT1 as an interactor of UBE2S. (b-c) Endogenous co-immunoprecipitation in EESC lysates employing antibodies specific to UBE2S or GLUT1, with subsequent immunoblot detection of reciprocal partners. (d) Assessments of glucose consumption, lactate output, and pyruvate generation in endometriosis-derived cells following enforced UBE2S expression. (e) Corresponding metabolic parameters in cells after UBE2S depletion. (f) Reintroduction of Flag-UBE2S into knockout EESCs and immunoblot evaluation of GLUT1 abundance. (g) Introduction of UBE2S-directed shRNA into EESCs and immunoblot quantification of GLUT1. (h-j) Metabolic readouts (glucose consumption, pyruvate, lactate) in EESCs after specified plasmid deliveries. (k-m) Parallel metabolic evaluations under different transfection conditions. (n-p) Further metabolic assays across indicated genetic manipulations. * $p < 0.05$, ** $p < 0.01$, *** $p < 0.001$, **** $p < 0.0001$

Staining via immunohistochemistry disclosed greater abundance of both UBE2S and GLUT1 within ectopic endometrial specimens relative to normal counterparts**.** Immunoblotting across 12 ectopic (EC), 12 eutopic (Eu), and 12 normal (NM) samples verified markedly heightened GLUT1 in EC tissues and derived EESCs versus Eu or NM controls ($p < 0.001$). As the primary facilitator of cellular glucose entry, GLUT1 plays a pivotal role in enhanced aerobic glycolysis. To determine if UBE2S governs this pathway in ectopic cells, impacts on glucose intake and production of lactate/pyruvate were examined. Enforced UBE2S substantially boosted these parameters **(Figure 3d)**, while its reduction diminished them **(Figure 3e).**

In UBE2S-deficient EESCs restored with varying UBE2S levels, GLUT1 protein showed notable elevation **(Figure 3f).** Parallel experiments with control or UBE2S shRNA in EESCs demonstrated a clear decline in GLUT1 upon UBE2S silencing (**Figure 3g**; $p < 0.05$). Dedicated GLUT1 suppression constructs were generated to probe dependency**.** Combined depletion of GLUT1 and UBE2S markedly lowered glucose intake and lactate/pyruvate output **(Figures 3h–j).** GLUT1 loss abrogated the metabolic elevation triggered by excess UBE2S **(Figures 3k–m),** whereas GLUT1 enrichment restored parameters diminished by UBE2S absence **(Figures 3n–p).** Collectively, these observations establish that UBE2S augments glycolytic activity and lactate generation in EESCs via control over GLUT1.

To evaluate UBE2S effects on metabolism amid controlled substrate availability, cultures were shifted to glucose-deprived media supplemented at 0, 5, or 25 mM glucose. Lactate yield was tracked in contexts of UBE2S gain or loss. Baseline cells exhibited glucose dose-responsive lactate rises. Added UBE2S amplified accumulation at every level**,** indicating enhanced flux. In contrast, UBE2S removal substantially curtailed output**.** Such patterns highlight UBE2S as a substrate-sensitive enhancer of glycolysis and lactate formation.

UBE2S diminishes K48-linked ubiquitin chains on GLUT1

As an E2 ubiquitin-conjugating component, UBE2S extends polyubiquitin modifications on targets, influencing their proteasomal clearance [15, 16]. To test involvement in GLUT1 turnover, proteasome blockade was applied via MG132 (10 μM, 8 h). In UBE2S-null EESCs, GLUT1 levels rose significantly post-inhibitor

exposure versus vehicle (**Figure 4a**; $p < 0.05$). No comparable shift occurred in wild-type UBE2S EESCs irrespective of treatment (**Figure 4a**; $p > 0.05$).

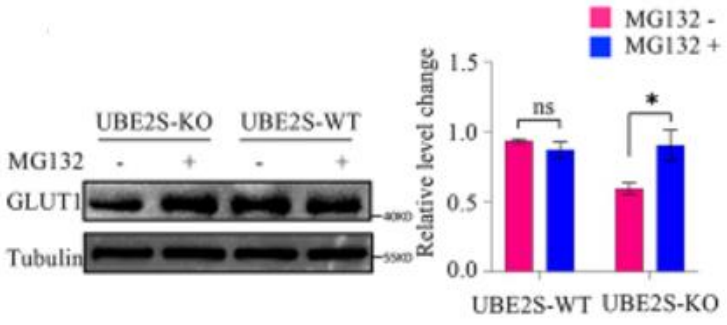

a)

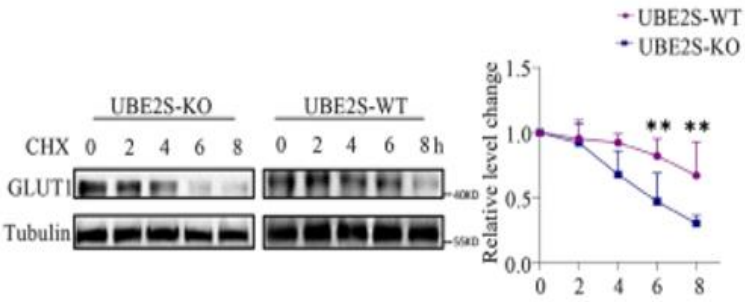

b)

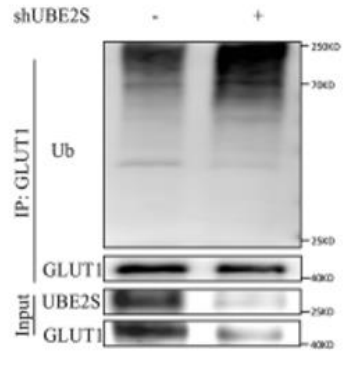

c)

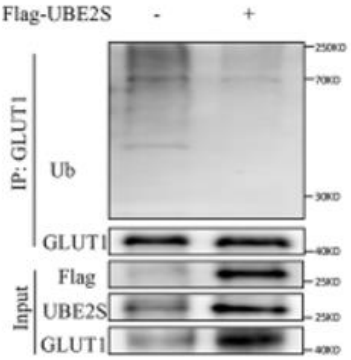

d)

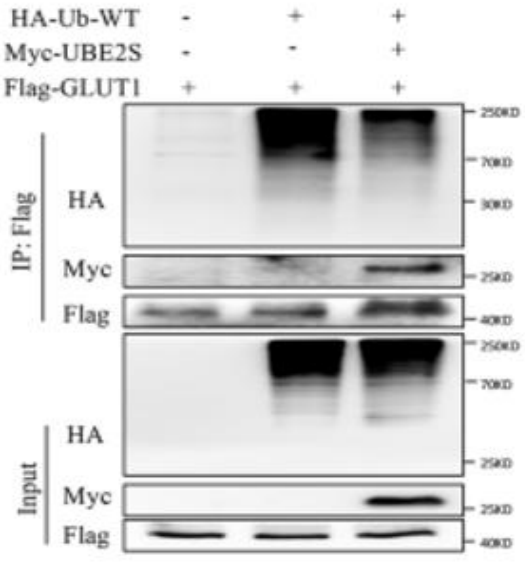

e)

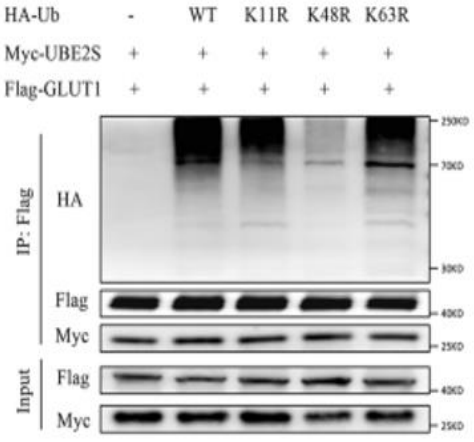

f)

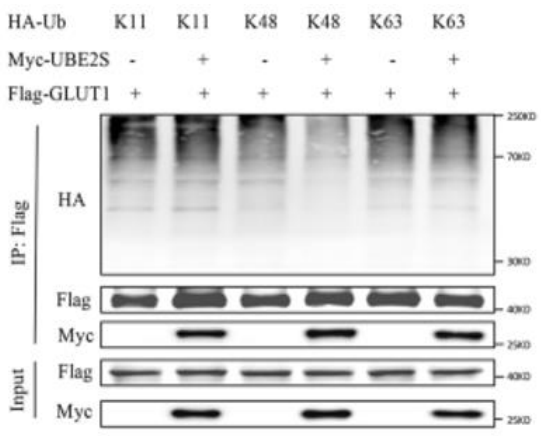

g)

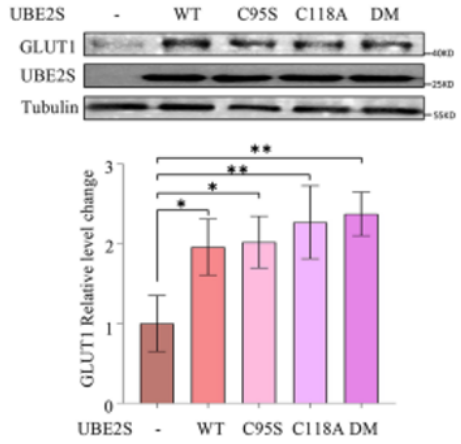

h)

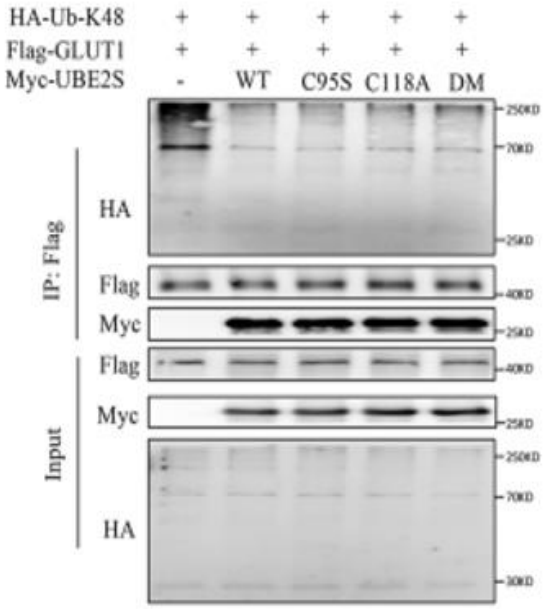

i)

Figure 4. UBE2S decreases K48-linked polyubiquitination of GLUT1. (a) EESCs UBE2S knockout (KO) and wild-type (WT) cells were treated with the proteasome inhibitor MG132 (10 μM, 8 h), and GLUT1 protein levels were evaluated by western blotting. (b) EESCs UBE2S-KO and WT cells were exposed to cycloheximide (CHX, 50 μg/mL) for varying durations, followed by western blot analysis of GLUT1 protein expression. (c) GLUT1 ubiquitination was examined in EESCs after transfection with shUBE2S. (d) GLUT1 ubiquitination was assessed in EESCs following Flag-UBE2S overexpression. (e) 293T cells were co-transfected with HA-Ub-WT, Myc-UBE2S, and Flag-GLUT1 plasmids, and GLUT1 ubiquitination was detected. (f) 293T cells were transfected with HA-Ub mutants (K11R, K48R, K63R), Flag-GLUT1, and Myc-UBE2S, and GLUT1 ubiquitination was evaluated by Co-IP. (g) 293T cells received Myc-UBE2S, Flag-GLUT1, and HA-Ub variants (K11-only, K48-only, K63-only), with GLUT1 ubiquitination analyzed via Co-IP. (h) UBE2S-KO 293T cells were transfected with Myc-UBE2S WT or its mutants (C95S, C118A, DM), and GLUT1 expression was determined by western blotting. (i) UBE2S-KO 293T cells were transfected with Myc-UBE2S WT or mutants (C95S, C118A, DM), together with Flag-GLUT1 and HA-Ub-K48, and GLUT1 ubiquitination was measured by Co-IP. * $p < 0.05$, ** $p < 0.01$, *** $p < 0.001$, **** $p < 0.0001$

We subsequently treated EESCs with the protein synthesis inhibitor cycloheximide (CHX, 50 µg/mL) and monitored GLUT1 protein levels at multiple time points. The data showed that, relative to UBE2S-WT EESCs, the half-life of GLUT1 was markedly shortened in UBE2S-KO cells after CHX exposure (**Figure 4b**; $p < 0.01$). These observations suggest that UBE2S enhances GLUT1 stability by suppressing its proteasome-mediated degradation, leading to higher GLUT1 levels in endometrial stromal cells during endometriosis.

To investigate if UBE2S modulates GLUT1 ubiquitination, we examined ubiquitination status in EESCs with either reduced or elevated UBE2S expression. Knockdown of UBE2S in EESCs resulted in elevated GLUT1 ubiquitination **(Figure 4c),** whereas UBE2S overexpression markedly lowered it **(Figure 4d).** In 293T cells co-transfected with Myc-UBE2S, HA-Ub-WT, and Flag-GLUT1, Co-IP analysis using anti-HA revealed that UBE2S overexpression substantially diminished GLUT1 ubiquitination **(Figure 4e).**

Given that K11-, K48-, and K63-linked ubiquitin chains can drive protein degradation or signaling [17], we explored linkage specificity in 293T cells using ubiquitin mutants (K11R, K48R, K63R). Results indicated that UBE2S influences GLUT1 ubiquitination primarily via the K48 pathway **(Figure 4f).** Further experiments in 293T cells overexpressing Myc-UBE2S, Flag-GLUT1, and single-lysine ubiquitin constructs (K11, K48, or K63) confirmed that UBE2S selectively suppresses K48-linked polyubiquitination of GLUT1 **(Figure 4g).** Thus, UBE2S specifically targets K48-linked chains rather than broadly affecting other linkage types.

UBE2S possesses E2 ubiquitin-conjugating activity and also functions as an E3 ligase [18, 19]. Its dual enzymatic roles rely on two cysteine residues (Cys95 and Cys118) within the UBC domain. To determine whether GLUT1 regulation by UBE2S requires E2 or E3 activity, we generated three mutants: C95S (loss of E2 activity), C118A (loss of E3 activity), and a double mutant (DM, loss of both). These, along with WT Myc-UBE2S, were introduced into UBE2S-KO 293T cells. Both WT and all mutants increased GLUT1 protein levels **(Figure 4h)** and effectively reduced GLUT1 ubiquitination **(Figure 4i).** These results imply that UBE2S-mediated K48 modification of GLUT1 is independent of its E2 or E3 catalytic functions.

UBE2S enlists the deubiquitinase USP10 to eliminate K48-linked polyubiquitination from GLUT1

Although UBE2S primarily acts as an E2 enzyme, our data indicate it may facilitate GLUT1 deubiquitination via an unidentified deubiquitinase, prompting deeper mechanistic studies. Mass spectrometry revealed USP10 as an interacting partner of UBE2S in EESCs. We therefore proposed that UBE2S recruits USP10 to cleave K48-linked ubiquitin chains from GLUT1 in EESCs. To test for direct binding, we conducted GST pull-down assays with recombinant proteins produced in E. coli: GST-UBE2S from pGEX-4T-1-UBE2S and His-USP10 from pET-24a(+)-USP10. Incubation showed that GST-UBE2S efficiently pulled down His-USP10, verified by anti-His immunoblotting, confirming direct interaction in vitro **(Figure 5a).** In EESC lysates, immunoprecipitation with anti-USP10 antibody and Protein A+G beads demonstrated that USP10 associates with both UBE2S and GLUT1 intracellularly **(Figure 5b).** Reciprocal immunoprecipitation using anti-UBE2S antibody further validated the UBE2S–USP10 interaction in EESCs **(Figure 5c).**

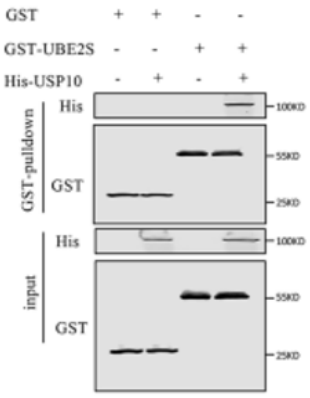

a)

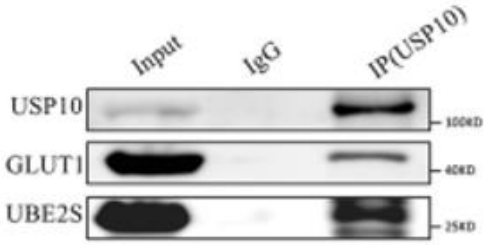

b)

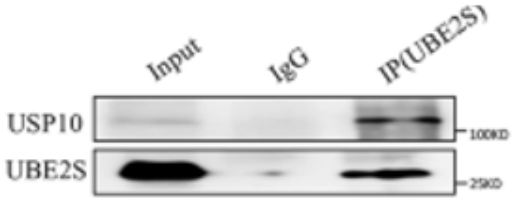
Input
IgG
IP(UBE2S)
USP10
UBE2S
100KD
25KD

c)

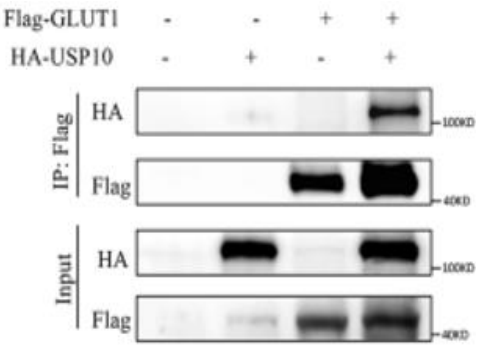
Flag-GLUT1 - - + +
HA-USP10 - + - +
IP: Flag
HA
Flag
Input
HA
Flag
100KD
40KD

d)

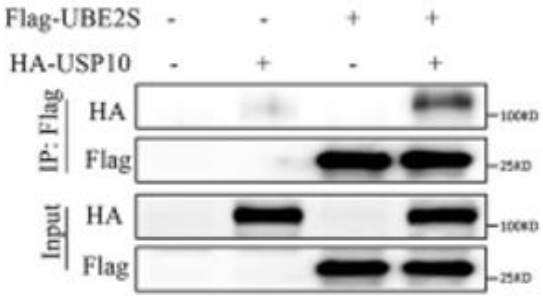
Flag-UBE2S - - + +
HA-USP10 - + - +
IP: Flag
HA
Flag
Input
HA
Flag
100KD
25KD

e)

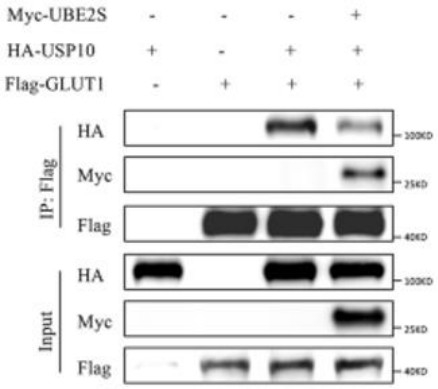
Myc-UBE2S - - - +
HA-USP10 + - + +
Flag-GLUT1 - + + +
IP: Flag
HA
Myc
Flag
Input
HA
Myc
Flag
100KD
25KD
40KD

f)

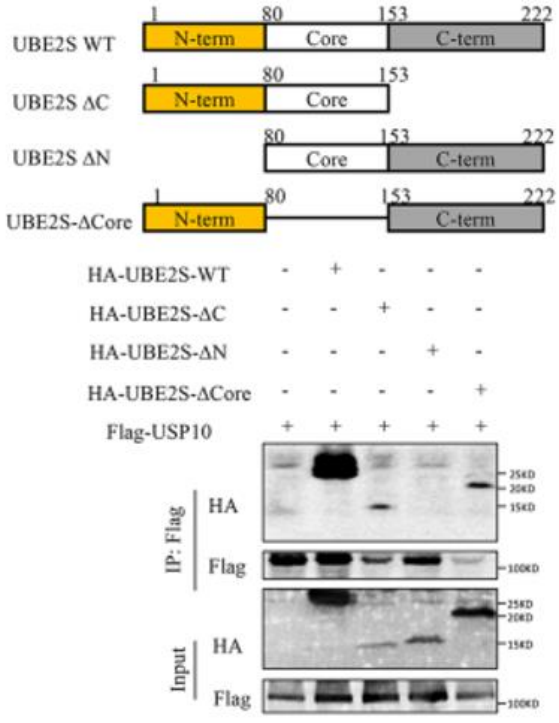
UBE2S WT 1 80 153 222 N-term Core C-term
UBE2S ΔC 1 80 153 N-term Core
UBE2S ΔN 80 153 222 Core C-term
UBE2S-ΔCore 1 80 153 222 N-term C-term
HA-UBE2S-WT - + - - -
HA-UBE2S-ΔC - - + - -
HA-UBE2S-ΔN - - - + -
HA-UBE2S-ΔCore - - - - +
Flag-USP10 + + + + +
IP: Flag
HA
Flag
Input
HA
Flag
25KD
20KD
15KD
100KD

g)

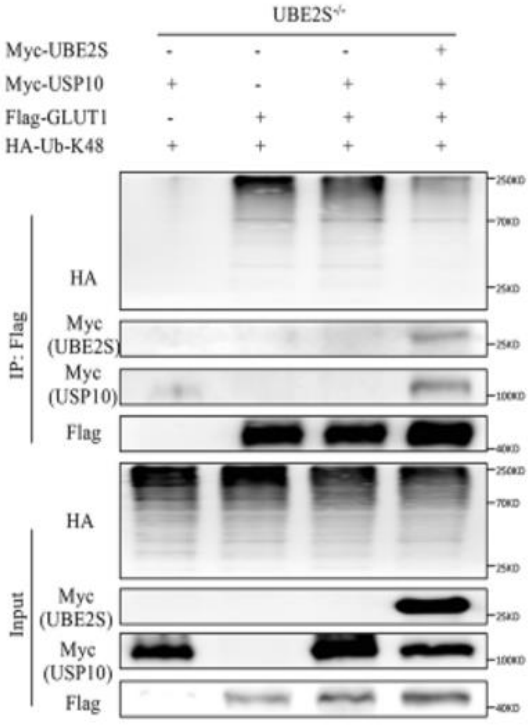
UBE2S-/-
Myc-UBE2S - - - +
Myc-USP10 + - + +
Flag-GLUT1 - + + +
HA-Ub-K48 + + + +
IP: Flag
HA
Myc (UBE2S)
Myc (USP10)
Flag
Input
HA
Myc (UBE2S)
Myc (USP10)
Flag
250KD
70KD
25KD
100KD
40KD

h)

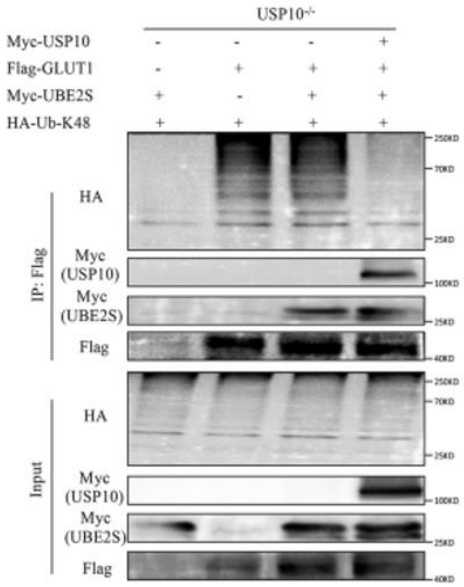

i)

Figure 5. UBE2S enlists USP10 to diminish K48-linked polyubiquitination of GLUT1. (a) Recombinant GST or GST-UBE2S was incubated with recombinant His-USP10. Pull-down was performed using glutathione agarose beads, and eluted samples were analyzed by SDS-PAGE and immunoblotting with anti-His antibody. Input and pull-down samples are displayed, with GST as a negative control. (b-c) Whole-cell lysates from EESCs were immunoprecipitated using monoclonal antibodies against USP10 or UBE2S, followed by western blotting to examine USP10 and UBE2S protein levels. (d-e) Co-IP performed on lysates from 293T cells transfected with the specified plasmids. (f) Co-IP on lysates from 293T cells transfected with the indicated plasmids. (g) Diagram of full-length UBE2S and its truncation mutants (top), along with Co-IP results showing binding of FLAG-tagged USP10 to HA-tagged wild-type or truncated UBE2S variants (ΔN, ΔC, and ΔCore) in HEK293T cells (bottom). (h) UBE2S-KO 293T cells transfected with Myc-UBE2S, Flag-GLUT1, Myc-USP10, and HA-Ub-K48 plasmids, followed by Co-IP on cell lysates. (i) USP10-KO 293T cells transfected with Myc-UBE2S, Flag-GLUT1, Myc-USP10, and HA-Ub-K48 plasmids, followed by Co-IP on cell lysates.

In 293T cells, co-expression of Flag-GLUT1 and HA-USP10 followed by Co-IP verified direct binding between GLUT1 and USP10 **(Figure 5d).** Likewise, co-expression of Flag-UBE2S and HA-USP10 confirmed binding between UBE2S and USP10 **(Figure 5e).** Additionally, triple transfection with Flag-GLUT1, Myc-UBE2S, and HA-USP10 in 293T cells showed that both Myc-UBE2S and HA-USP10 co-precipitated with Flag-GLUT1, reinforcing the association among GLUT1, USP10, and UBE2S **(Figure 5f).**

To determine which regions of UBE2S mediate its binding to USP10, we introduced three HA-tagged truncation mutants (ΔC, ΔN, and ΔCore) along with Flag-USP10 into 293T cells and conducted Co-IP. Data showed that USP10 bound to wild-type UBE2S, ΔC, and ΔCore mutants, but not to the ΔN mutant **(Figure 5g).** This indicates that the N-terminal region of UBE2S is critical for USP10 interaction.

To examine the cooperative effects of UBE2S and USP10 on K48-linked ubiquitination of GLUT1, we first tested USP10–GLUT1 association. In UBE2S-KO 293T cells co-transfected with Flag-GLUT1, Myc-UBE2S, and Myc-USP10, USP10 failed to bind GLUT1 without UBE2S, but associated with GLUT1 when UBE2S was present **(Figure 5h).** In USP10-KO 293T cells transfected with Flag-GLUT1, Myc-UBE2S, and Myc-USP10, UBE2S alone did not lower K48-linked ubiquitination of GLUT1, whereas combined expression of UBE2S and USP10 markedly reduced it **(Figure 5i).** These results indicate that neither protein suffices independently for K48 deubiquitination of GLUT1; both are required concurrently. UBE2S acts as a scaffold via its N-terminal domain to assemble a ternary complex

with GLUT1 and USP10, thereby removing K48-linked chains from GLUT1 and preserving its protein stability.

UBE2S promotes glycolysis and drives M2 macrophage polarization

UBE2S shows elevated immune scores in breast cancer, glioma, bladder cancer, and liver cancer, reflecting close ties to the tumor immune microenvironment [20, 21]. Excessive M2 macrophage infiltration characterizes the chronic inflammation in endometriosis (EM). To assess UBE2S impact on M2 polarization in EM, THP-1 cells were differentiated into M0 macrophages with PMA and then co-cultured with differentially treated EESCs. Macrophages were harvested to evaluate M2 markers **(Figure 6a).** Results demonstrated that, relative to co-culture with control EESCs, macrophages exposed to UBE2S-overexpressing EESCs displayed markedly higher mRNA levels of CD163 **(Figure 6b),** Arg-1 **(Figure 6c),** and CD206 **(Figure 6d).** Furthermore, GLUT1 knockdown in EESCs abrogated the UBE2S-induced increase in M2 polarization **(Figures 6b–d).** Protein-level confirmation was obtained via western blotting **(Figure 6e).**

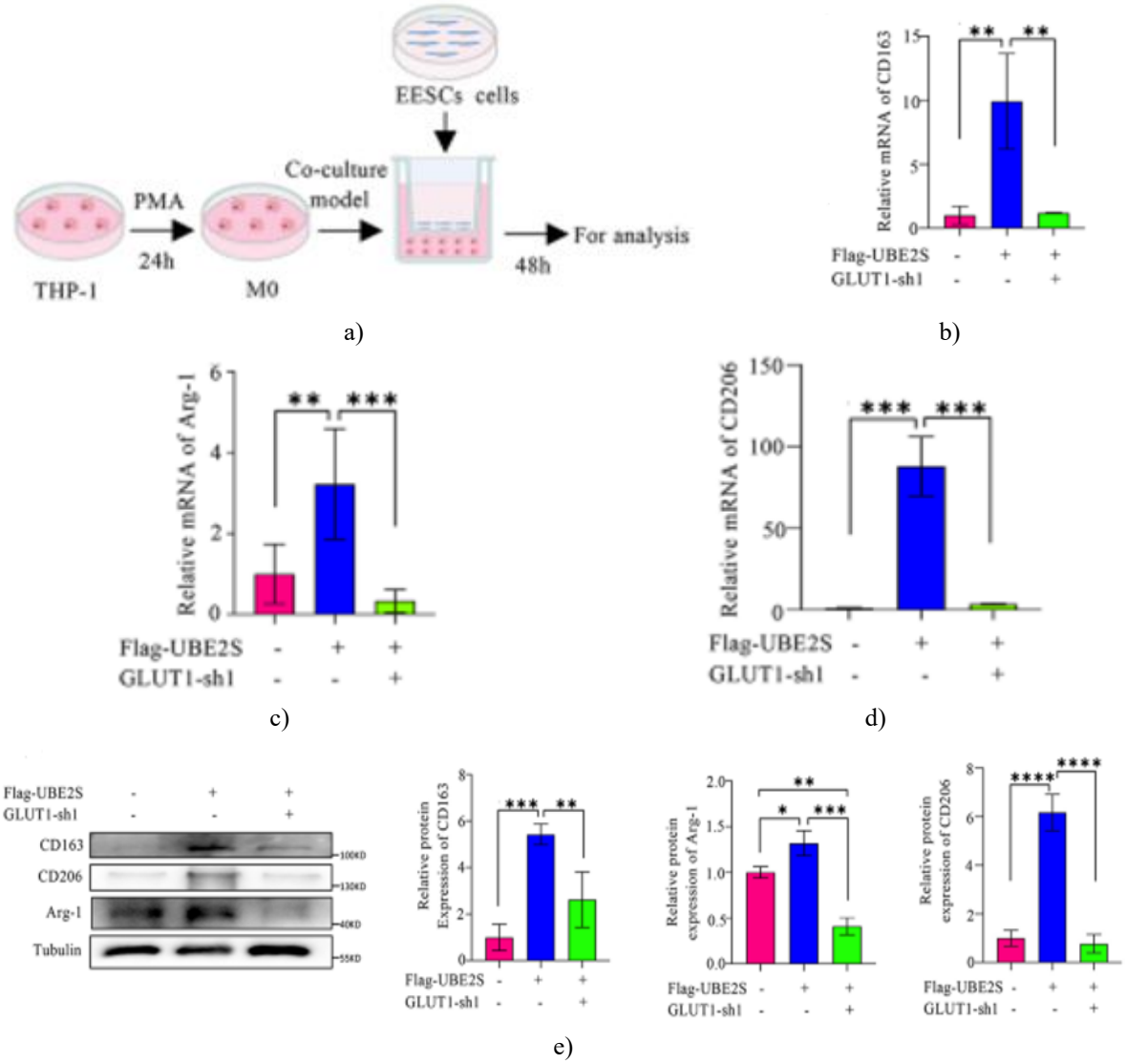

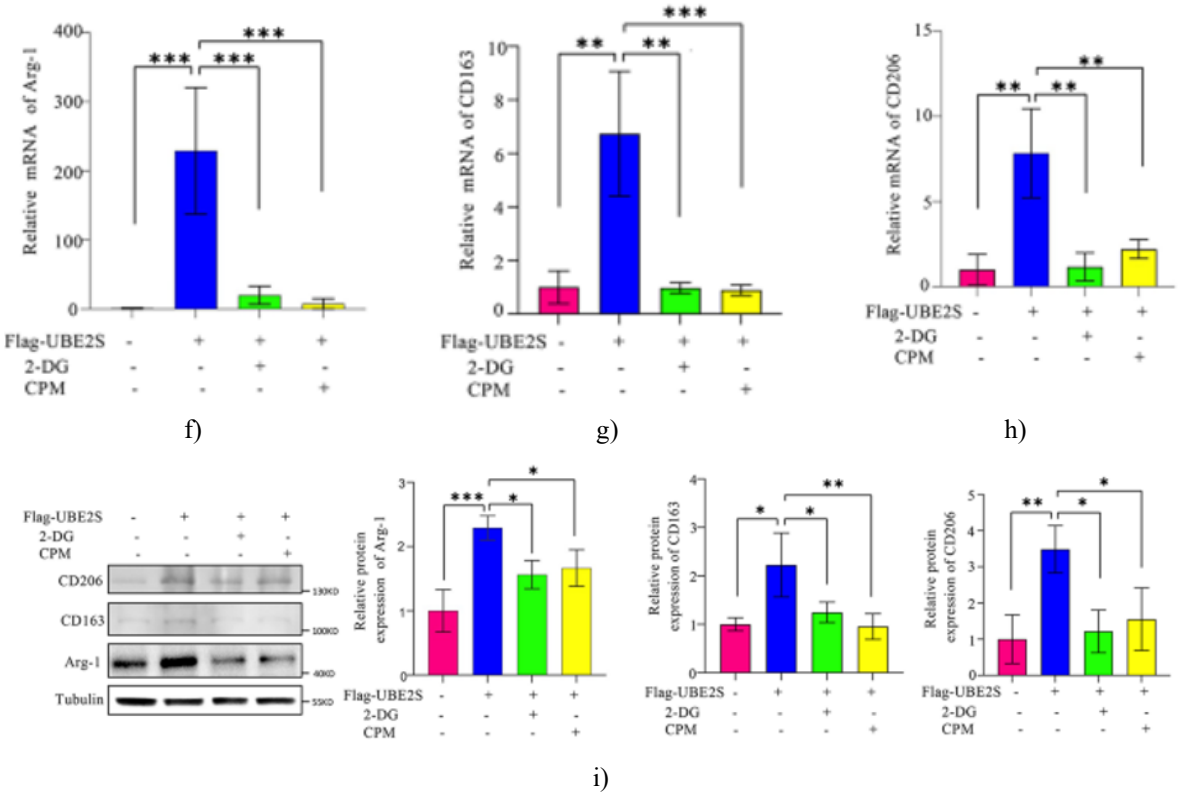

Figure 6. Elevated UBE2S levels in EESCs stimulate glycolytic activity and favor M2-type macrophage differentiation. (a) Illustration of the co-culture setup. (b-d) Quantitative RT-PCR quantification of CD163, CD206, and Arg-1 transcript abundance in macrophages following 48 h co-culture with EESCs harboring various transfections. (e) Immunoblot detection of CD163, CD206, and Arg-1 proteins in macrophages from co-cultures with differently transfected EESCs. (f-h) UBE2S-overexpressing EESCs were exposed to 2-DG or CPM for 24 h; the resulting conditioned media (CM) were harvested and applied to M0 macrophages. Quantitative RT-PCR evaluation of CD163, CD206, and Arg-1 transcripts in treated macrophages. (i) Parallel setup as above, with immunoblot assessment of CD163, CD206, and Arg-1 proteins in macrophages. * $p < 0.05$, ** $p < 0.01$, *** $p < 0.001$, **** $p < 0.0001$

Cephalomannine (CPM), a small-molecule agent, downregulates UBE2S protein abundance [22]. EESCs transfected with Flag-UBE2S (labeled OE-UBE2S-EESCs) were shifted to serum-free conditions for 24 h, then exposed to vehicle (DMSO), 1 mM 2-deoxyglucose (2-DG), or 100 μM CPM for 24 h. Media were renewed, culture extended another 24 h, and supernatants collected, diluted 1:1 with fresh media, then used to stimulate M0 macrophages for 48 h prior to M2 marker analysis. Inclusion of 2-DG or CPM during OE-UBE2S-EESC conditioning strongly suppressed subsequent macrophage M2 differentiation, evident at both transcript and protein levels **(Figures 6f–i),** achieving statistical significance.

To establish lactate as a critical downstream component in UBE2S/GLUT1-orchestrated M2 differentiation, exogenous sodium lactate rescue studies were performed. M0 macrophages co-cultured with EESCs bearing UBE2S or GLUT1 shRNA received vehicle or 10 mM sodium lactate. Immunoblotting showed a marked decline in M2-associated proteins (CD206, Arg1, CD163) upon either knockdown, but partial recovery of these proteins occurred with lactate addition**.** This supports lactate's role as a key executor in the UBE2S/GLUT1 pathway driving M2 polarization.

Overall, these data establish that UBE2S augments GLUT1 abundance, accelerates glycolysis within EESCs, and thereby sustains M2 macrophage presence in endometriotic tissues. Disruption of UBE2S function or glycolytic flux in EESCs curbs M2 differentiation at lesion sites.

M2 macrophage shifts in endometriotic tissues influence EESC functional properties

Endometriosis progresses as a fibrosing disorder featuring tissue rigidity, primarily from abundant extracellular matrix buildup during fibrotic remodeling [23]. Evidence links endogenous macrophage phenotypes to remodeling dynamics in endometriosis, where M2 cells correlate positively with fibrotic extent. These M2 cells produce TGF-β1, fostering fibrogenesis in endometrial lineages [24]. Heightened stromal cell motility and invasiveness hallmark fibrotic progression. We quantified TGF-β1 and observed substantial upregulation in macrophages after exposure to UBE2S-overexpressing EESCs (OE-UBE2S-EESCs), while 2-DG or CPM exposure notably suppressed it.

Having examined stromal impact on macrophages, we reversed the direction to probe macrophage influence on endometriotic stromal behavior. Macrophages co-cultured for 48 h with either UBE2S-overexpressing EESCs (M0-UBE2S) or vector-control EESCs (M0-NC), followed by stromal cell removal and 24 h further incubation in fresh serum-free media. Harvested supernatants, diluted 1:1 with serum-free media to yield conditioned medium (CM), were applied to naive EESCs **(Figure 7a).** M0-UBE2S-derived CM potently augmented EESC proliferative capacity **(Figures 7b–c)** and motility **(Figure 7d).** Such gains were largely abolished by prior 2-DG exposure in the M0-UBE2S arm **(Figures 7b–d)**, yielding significant reductions. Conversely, CM from macrophages co-cultured with UBE2S-depleted EESCs (M0-sh-UBE2S) impaired EESC proliferation and migration, effects partially overridden by 10 mmol/L lactate supplementation to the CM (**Figures 7e–g**; $p < 0.05$).

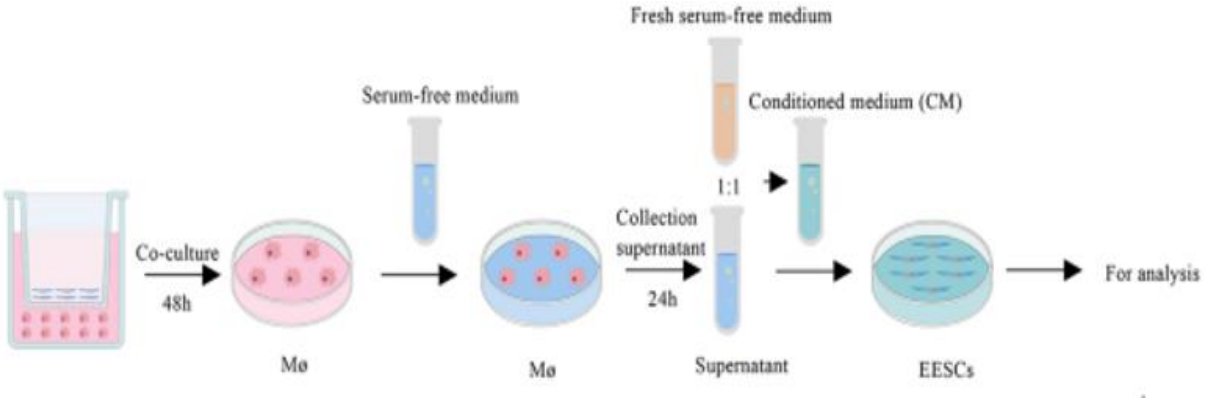

a)

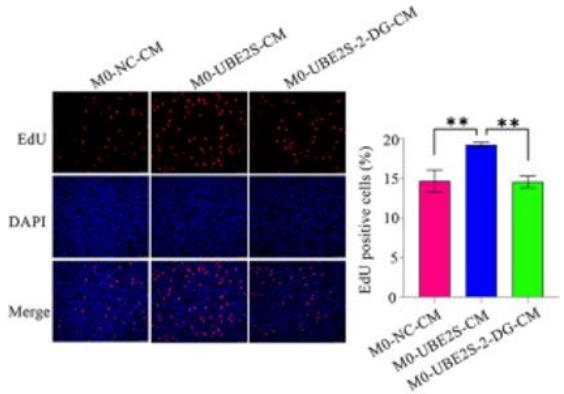

b)

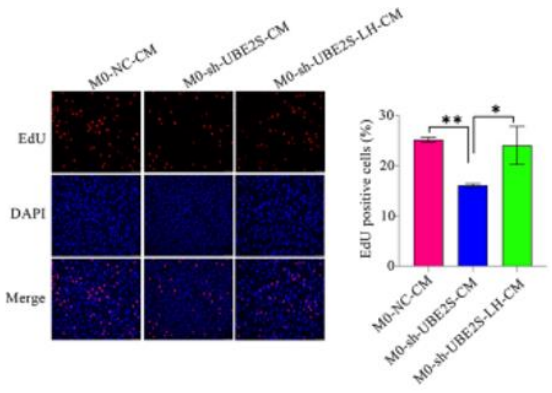

e)

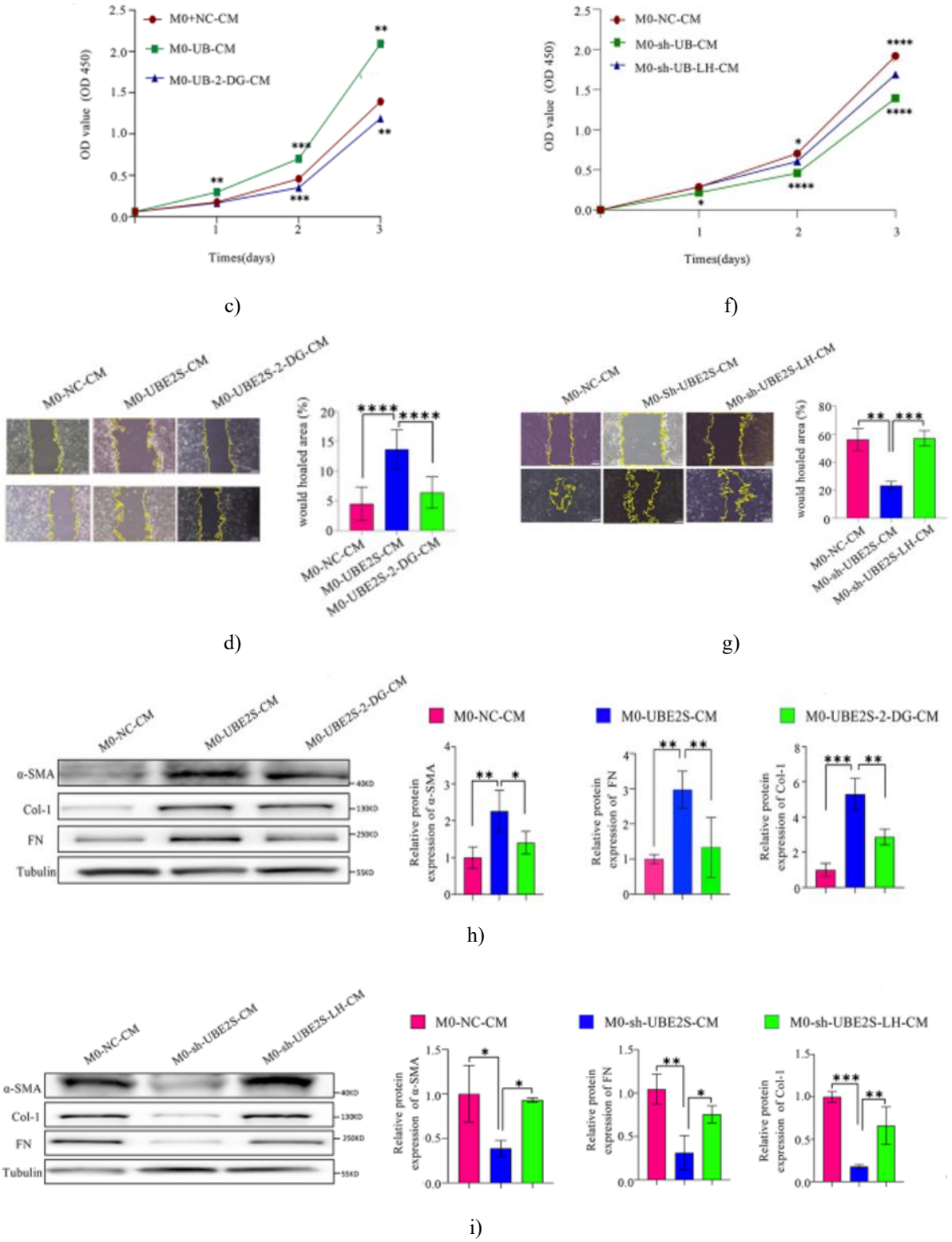

Figure 7. M2-type macrophages drive cell proliferation, motility, and fibrotic changes in endometriotic stromal cells. (a) Schematic overview of conditioned medium (CM) treatment applied to EESCs. (b) EdU incorporation assay measuring EESC proliferative activity. (c) CCK-8 assay quantifying EESC proliferative rates. (d) Wound-healing scratch test examining EESC migratory capacity following CM exposure. (e) EdU incorporation assay

evaluating EESC proliferative response. (f) CCK-8 assay determining EESC growth rates. (g) Wound-healing scratch test assessing EESC motility after CM application. (h) Immunoblot detection of fibrotic tissue remodeling (FMT) indicators (α-SMA, FN, Col-1) in EESCs exposed to CM for 48 h. (i) Immunoblot examination of FMT indicators in EESCs after 48 h CM incubation. * $p < 0.05$, ** $p < 0.01$, *** $p < 0.001$, **** $p < 0.0001$

Subsequent analysis focused on fibrotic remodeling markers across EESC treatment conditions. Data showed that CM from M0-UBE2S co-cultures markedly elevated α-SMA, Col-1, and FN protein abundance in recipient EESCs **(Figure 7h)**. Exposure to 2-DG notably attenuated this fibrotic induction **(Figure 7h).** In contrast, CM from M0-sh-UBE2S systems lowered expression of these markers, while lactate supplementation to the CM largely counteracted the decline **(Figure 7i),** yielding significant statistical outcomes. Collectively, these observations reveal that M2 macrophages, induced by UBE2S-high EESCs, accelerate stromal proliferation, motility, and fibrotic remodeling in endometriosis.

To confirm CPM selectivity toward UBE2S, computational docking was conducted against a set of proteins involved in ubiquitination, glycolytic pathways, and fibrogenesis [25, 26]. Results highlighted strong binding preference for UBE2S, whereas substantially weaker affinities (higher ΔG values) were calculated for alternative targets including ubiquitin enzymes (UBE2C, UBE2D1, USP10, USP7, OTUB1), glycolytic components (HK2, PFKFB3, PKM2, LDHA), and fibrosis-linked kinases (TGF-βR1, SMAD3, MAPK1, JNK1, mTOR), implying minimal off-target risks.

Rescue studies in UBE2S-deficient EESCs clarified the CPM mechanism. Genetic ablation of UBE2S alone decreased lactate output, and CPM failed to impose additional suppression in this knockout context, confirming UBE2S dependency for CPM-mediated glycolytic blockade**.** Antifibrotic specificity was tested via macrophage-EESC co-culture **(Figure 7a).** CM harvested from macrophage interactions with UBE2S-KO (M0-KO) or wild-type (M0-WT) EESCs was transferred to fresh EESCs. Immunoblotting demonstrated that M0-KO-derived CM substantially diminished fibrotic markers (α-SMA, Col-1, FN) relative to M0-WT CM**.** CPM exposure in UBE2S-absent co-cultures produced no further marker reduction, whereas CPM application to wild-type systems potently suppressed fibrosis indicators compared to vehicle controls, with clear statistical significance**.** Thus, CPM antifibrotic action relies explicitly on UBE2S presence, reinforcing targeted modulation of glycolysis-fibrosis axes.

UBE2S facilitates endometriosis progression in vivo

A global UBE2S knockout (UBE2S−/−) mouse line was generated to probe UBE2S contributions to endometrial function in living organisms. Homozygous knockout females exhibited sharply reduced fertility, prompting the use of UBE2S−/− males crossed with heterozygous females for propagation. Endometriosis lesions were induced using endometrial fragments from UBE2S−/− donors to assess in vivo consequences **(Figure 8a).** Lesion dimensions were notably smaller in knockout recipients **(Figure 8b).** Quantitative assessment of total lesion volume and mass across cohorts confirmed substantial growth restraint in the UBE2S-deficient group **(Figures 8c-d).** Hence, systemic UBE2S depletion effectively impedes endometriosis establishment and expansion in murine models.

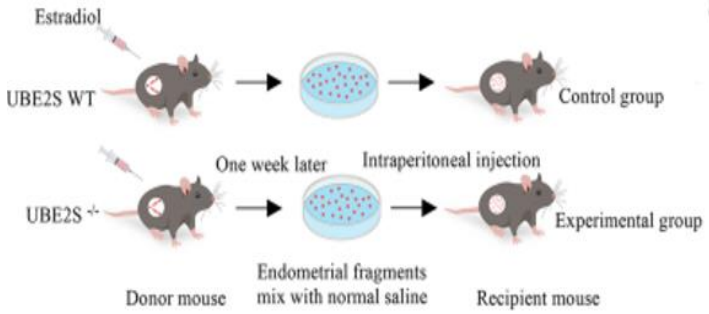

a)

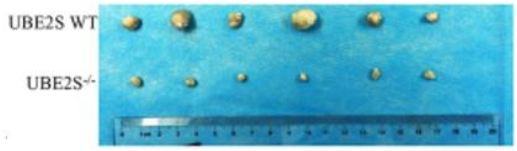
UBE2S WT
UBE2S-/-

b)

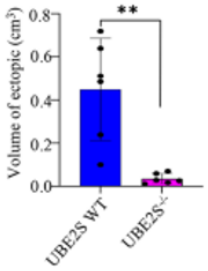
Volume of ectopic (cm³)
0.8
0.6
0.4
0.2
0.0
**
UBE2S WT
UBE2S-/-

c)

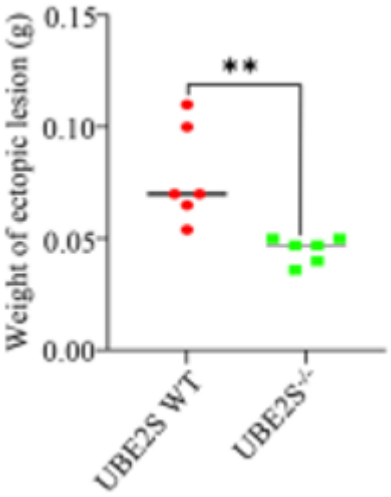
Weight of ectopic lesion (g)
0.15
0.10
0.05
0.00
**
UBE2S WT
UBE2S-/-

d)


Control
CPM

f)

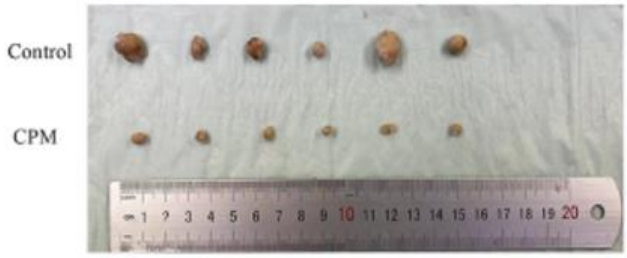
Control
CPM

g)

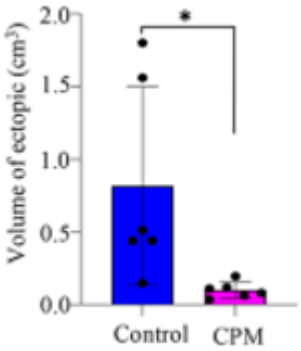
Volume of ectopic (cm³)
2.0
1.5
1.0
0.5
0.0
*
Control
CPM

h)

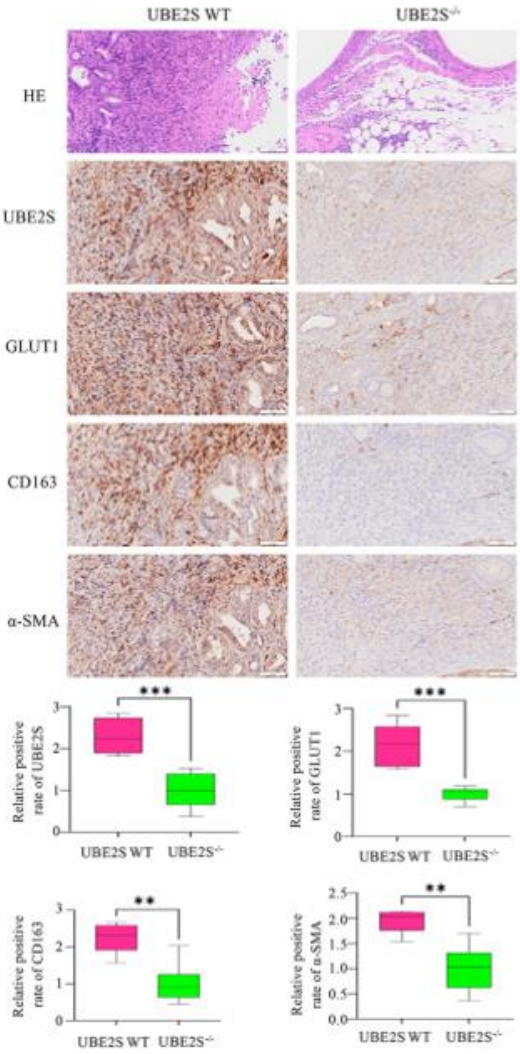

e)

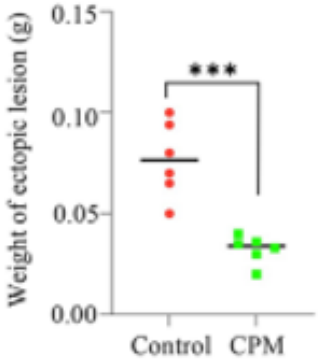

i)

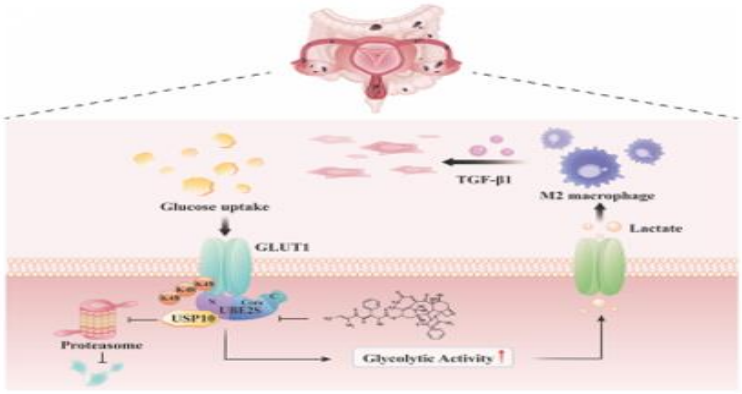

j)

Figure 8. UBE2S drives endometriosis progression in animal models. (a) Generation of the UBE2S knockout mouse model for endometriosis induction. (b-d) Body weight measurements and endometriotic lesion volumes in treatment (n = 6) and control (n = 6) cohorts post-lesion excision. (e) Hematoxylin-eosin (H&E, 10x) and immunohistochemistry (IHC, 20x) staining for UBE2S, GLUT1, CD163, and α-SMA (scale bar = 50 μm).

Staining intensity quantified via ImageJ analysis. (f) Administration of CPM in the C57BL/6J endometriosis model. (g) Representative photographs of the most prominent ectopic implants per animal. (h-i) Quantification of ectopic lesion volume (h) and mass (i). (j) Overview diagram illustrating UBE2S-orchestrated metabolic shifts and immune regulation in endometriosis. * $p < 0.05$, ** $p < 0.01$, *** $p < 0.001$

IHC staining was subsequently conducted to measure UBE2S and GLUT1 abundance. Lesions from the knockout group displayed markedly lower UBE2S and GLUT1 expression compared to controls (**Figure 8e**; $p < 0.001$). Markers for fibrosis (α-SMA) and M2 macrophages (CD163) were also diminished, supporting UBE2S's role in fostering M2 polarization and fibrotic processes during in vivo endometriosis advancement (**Figure 8e**; $p < 0.01$). Immunofluorescence on lesion sections from wild-type and UBE2S$^{-/-}$ mice further revealed that in wild-type tissues, GLUT1-positive stromal cells were closely associated with CD163-positive M2 macrophages. This association was greatly attenuated in knockout lesions, which showed reduced GLUT1 and fewer CD163^{+} infiltrates**.** Quantification confirmed decreased CD163^{+} cell density in knockout samples. Likewise, wild-type lesions featured enriched α-SMA^{+} fibroblasts near GLUT1^{+} areas, indicative of ongoing fibrosis, whereas knockout lesions exhibited lower GLUT1 and α-SMA signals**.** Quantitative data corroborated these observations. Together, these in vivo findings substantiate UBE2S's promotion of M2 macrophage recruitment and fibrotic changes via GLUT1-mediated pathways.

To test the therapeutic potential of the UBE2S inhibitor CPM in vivo, an endometriosis model was induced in C57BL/6J mice **(Figure 8f).** The treatment arm received weekly intraperitoneal CPM (10 mg/kg). After four weeks, ectopic tissues were harvested and evaluated **(Figure 8g).** Treatment resulted in significantly smaller lesion volumes and weights relative to vehicle controls **(Figures 8h-i)**. These data highlight CPM's potent in vivo efficacy against endometriosis through UBE2S inhibition.

Glycolytic dysregulation in endometriotic tissues is well-documented [27, 28], yet the underlying molecular drivers remain poorly defined. Transcriptomic profiling revealed substantial UBE2S upregulation in endometriotic stromal cells (EESCs). Prior research linked UBE2S to metabolic reprogramming in tumors, such as stabilizing VHL in hepatocellular carcinoma to indirectly bolster HIF-1α and upregulate glycolytic genes, thereby increasing glucose uptake and lactate output under hypoxia [10]. In contrast, our work uncovered a distinct mechanism: UBE2S recruits USP10 to catalyze K48-linked deubiquitination of GLUT1, preventing its degradation and enhancing stability. This pathway likely operates independently of severe hypoxia, given the partial oxygenation in endometriotic lesions. Functional assays confirmed that UBE2S-stabilized GLUT1 markedly boosts glucose uptake and glycolytic rates, pushing EESCs toward a hyper-glycolytic state. This represents novel evidence for UBE2S's direct involvement in glycolytic control, broadening insights into metabolic aberrations in endometriosis.

UBE2S typically exerts pathogenic effects via its E2/E3 enzymatic activities, targeting substrates for ubiquitination. Examples include K11-linked modification of APC/C to hasten cell cycle progression [29] and stabilization of β-catenin to enhance Wnt signaling and metastasis in colorectal cancer [30]. Emerging evidence indicates UBE2S can also recruit deubiquitinases like USP15 for opposing functions [19]. Our findings extend this dual role, demonstrating that UBE2S engages USP10 via its N-terminal region to facilitate K48-linked deubiquitination of GLUT1. USP10 requires UBE2S to form a functional complex for this activity. This discovery unveils a previously unrecognized deubiquitination-dependent role for UBE2S in GLUT1 regulation, enriching its multifaceted biological profile.

Endometriosis is a persistent inflammatory condition with profound immune microenvironment alterations [31]. M2 macrophages predominate in lesions, fueling chronic inflammation and fibrosis. We observed that UBE2S-enhanced GLUT1 stability elevates glycolytic output in EESCs, leading to lactate accumulation that promotes M2 polarization. Lactate influences macrophage phenotype via HIF-1α and STAT3 pathways [5, 32]. Additional experiments showed that UBE2S-driven GLUT1 overexpression raised lactate and induced M2 markers (CD206, Arg-1, IL-10). Suppression of UBE2S or glycolytic inhibition reversed these changes, underscoring the pathway's critical role in macrophage reprogramming.

Persistent inflammation and scarring in endometriosis (EM) lesions play a central role in driving disease advancement and relapse [33-35]. M2-type macrophages

release TGF-β1 and PDGF, which stimulate fibroblasts and drive their transformation into myofibroblasts via the TGF-β1/Smad pathway, thereby hastening tissue fibrosis [4, 36, 37]. Experiments conducted in vitro and in animal models showed that UBE2S-driven polarization of M2 macrophages facilitated the shift of EM stromal fibroblasts toward a myofibroblast phenotype, with elevated levels of α-SMA and Col1. Administration of the UBE2S inhibitor CPM markedly suppressed this process, indicating that UBE2S could serve as a promising target for treating fibrosis associated with EM. It is worth noting that, although UBE2S knockout impairs fertility in female mice, this effect stems mainly from early embryonic death due to APC/C inactivation and meiotic blockage, not from hormonal disruption or ovarian defects [38]. In our study, UBE2S–/– females exhibited no alterations in sexual development, estrous cycle patterns, or ovarian follicle reserve. Additionally, to minimize hormonal fluctuations during model establishment, both recipient and donor mice underwent uniform estrogen priming and cycle synchronization. Such standardization ensures that the observed fibrotic and metabolic changes are not influenced by hormonal or developmental variations, but instead highlight the direct involvement of UBE2S in mature endometrial function.

Nevertheless, certain limitations exist in this work. The investigation relied predominantly on cellular and murine models, and validation using human patient specimens is required to strengthen its clinical relevance. The metabolic shift driven by GLUT1 might engage additional downstream cascades, such as the PI3K/Akt/mTOR pathway [39, 40]. Subsequent research should explore these signaling networks in greater detail. While in silico docking and rescue experiments in UBE2S-knockout cells support CPM's selectivity, comprehensive profiling of deubiquitinases or kinases was not performed. Predictive computational models cannot completely replicate intracellular binding behavior. Future chemical proteomics approaches could verify CPM's precise targets in physiological settings.

Conclusion

In summary, the present study reveals a previously unrecognized pathway in which UBE2S-dependent deubiquitination of GLUT1 modulates glucose uptake, immune milieu, and fibrogenesis in EM, positioning UBE2S as a candidate therapeutic target **(Figure 8j).** These results provide fresh perspectives on EM pathogenesis and establish a conceptual basis for upcoming therapeutic strategies in patients.

Acknowledgments: None

Conflict of Interest: None

Financial Support: None

Ethics Statement: None

References

1. Lu C, Qiao P, Fu R, Wang Y, Lu J, Ling X, et al. Phosphorylation of PFKFB4 by PIM2 promotes anaerobic Glycolysis and cell proliferation in endometriosis. Cell Death Dis. 2022;13(9):790–801.
2. Esfandiari F, Chitsazian F, Jahromi MG, Favaedi R, Bazrgar M, Aflatoonian R, et al. HOX cluster and their cofactors showed an altered expression pattern in eutopic and ectopic endometriosis tissues. Reprod Biol Endocrinol. 2021;19(1):132–42.
3. Ivashkiv LB. The hypoxia-lactate axis tempers inflammation. Nat Rev Immunol. 2020;20(2):85–6.
4. Nishimoto-Kakiuchi A, Sato I, Nakano K, Ohmori H, Kayukawa Y, Tanimura H, et al. A long-acting anti-IL-8 antibody improves inflammation and fibrosis in endometriosis. Sci Transl Med. 2023;15(684):eabq5858.
5. Gou Y, Wang H, Wang T, Wang H, Wang B, Jiao N, et al. Ectopic endometriotic stromal cells-derived lactate induces M2 macrophage polarization via Mettl3/Trib1/ERK/STAT3 signalling pathway in endometriosis. Immunology. 2023;168(3):389–402.
6. Ling X, Lu J, Wang X, Liu L, Liu L, Wang Y, et al. Ovarian tumorB1-mediated heat shock transcription factor 1 deubiquitination is critical for Glycolysis and development of endometriosis. iScience. 2022;25(11):105363.
7. Popovic D, Vucic D, Dikic I. Ubiquitination in disease pathogenesis and treatment. Nat Med. 2014;20(11):1242–53.
8. Jung CR, Hwang KS, Yoo J, Cho WK, Kim JM, Kim WH, et al. E2-EPF UCP targets pVHL for degradation and associates with tumor growth and metastasis. Nat Med. 2006;12(7):809–16.
9. Han Z, Xu L, Wang A, Wang B, Liu Q, Liu H, et al. UBE2S facilitates glioblastoma progression through activation of the NF-kappaB pathway via attenuating

K11-linked ubiquitination of AKIP1. Int J Biol Macromol. 2024;278(Pt 1):134426.
10. Zhang R, Li C, Zhang S, Kong L, Liu Z, Guo Y, et al. UBE2S promotes Glycolysis in hepatocellular carcinoma by enhancing E3 enzyme-independent polyubiquitination of VHL. Clin Mol Hepatol. 2024;30(4):771–92.
11. De Leo A, Ugolini A, Yu X, Scirocchi F, Scocozza D, Peixoto B, et al. Glucose-driven histone lactylation promotes the immunosuppressive activity of monocyte-derived macrophages in glioblastoma. Immunity. 2024;57(5):1105–23.
12. Colegio OR, Chu NQ, Szabo AL, Chu T, Rhebergen AM, Jairam V, et al. Functional polarization of tumour-associated macrophages by tumour-derived lactic acid. Nature. 2014;513(7519):559–63.
13. Ren L, Xu B, Xu J, Li J, Jiang J, Ren Y, et al. A machine learning model to predict survival and therapeutic responses in multiple myeloma. Int J Mol Sci. 2023;24(7):6683–700.
14. Aran D, Hu Z, Butte AJ. xCell: digitally portraying the tissue cellular heterogeneity landscape. Genome Biol. 2017;18(1):220–34.
15. Pickart CM. Back to the future with ubiquitin. Cell. 2004;116(2):181–90.
16. Trulsson F, Akimov V, Robu M, van Overbeek N, Berrocal DAP, Shah RG, et al. Deubiquitinating enzymes and the proteasome regulate Preferential sets of ubiquitin substrates. Nat Commun. 2022;13(1):2736–53.
17. Xu P, Duong DM, Seyfried NT, Cheng D, Xie Y, Robert J, et al. Quantitative proteomics reveals the function of unconventional ubiquitin chains in proteasomal degradation. Cell. 2009;137(1):133–45.
18. Lim JH, Shin HW, Chung KS, Kim NS, Kim JH, Jung HR, et al. E2-EPF UCP possesses E3 ubiquitin ligase activity via its cysteine 118 residue. PLoS ONE. 2016;11(9):e0163710.
19. Huang L, Liu H, Zhang K, Meng Q, Hu L, Zhang Y, et al. Ubiquitin-Conjugating enzyme 2S enhances viral replication by inhibiting type I IFN production through recruiting USP15 to deubiquitinate TBK1. Cell Rep. 2020;32(7):108044.
20. Yue H, Wang J, Hou S, Zhang M. As a potential predictor of pan-cancer, UBE2S is related to tumor-associated macrophage infiltration. Future Oncol. 2023;19(29):1973–90.
21. Qiu L, Wang Y, Li Z, Tu Z, Liu H. The landscape of UBE2S in hepatocellular carcinoma: prognostic significance, immuno-oncology feature and drug response. Genes Dis. 2023;10(2):363–5.
22. Peng S, Chen X, Huang C, Yang C, Situ M, Zhou Q, et al. UBE2S as a novel ubiquitinated regulator of p16 and beta-catenin to promote bone metastasis of prostate cancer. Int J Biol Sci. 2022;18(8):3528–43.
23. Muraoka A, Suzuki M, Hamaguchi T, Watanabe S, Iijima K, Murofushi Y, et al. Fusobacterium infection facilitates the development of endometriosis through the phenotypic transition of endometrial fibroblasts. Sci Transl Med. 2023;15(700):eadd1531.
24. Bokhari AA, Lee LR, Raboteau D, Hamilton CA, Maxwell GL, Rodriguez GC, et al. Progesterone inhibits endometrial cancer invasiveness by inhibiting the TGFbeta pathway. Cancer Prev Res (Phila). 2014;7(10):1045–55.
25. McKinnon BD, Kocbek V, Nirgianakis K, Bersinger NA, Mueller MD. Kinase signalling pathways in endometriosis: potential targets for non-hormonal therapeutics. Hum Reprod Update. 2016;22(3):382–403.
26. Zhang M, Xu T, Tong D, Li S, Yu X, Liu B, et al. Research advances in endometriosis-related signaling pathways: A review. Biomed Pharmacother. 2023;164:114909.
27. Garcia-Gomez E, Vazquez-Martinez ER, Reyes-Mayoral C, Cruz-Orozco OP, Camacho-Arroyo I, Cerbon M. Regulation of inflammation pathways and inflammasome by sex steroid hormones in endometriosis. Front Endocrinol (Lausanne). 2019;10:935–52.
28. Chen Q, Jiao Y, Yin Z, Fu X, Guo S, Zhou Y, et al. Establishment of a novel glycolysis-immune-related diagnosis gene signature for endometriosis by machine learning. J Assist Reprod Genet. 2023;40(5):1147–61.
29. Williamson A, Wickliffe KE, Mellone BG, Song L, Karpen GH, Rape M. Identification of a physiological E2 module for the human anaphase-promoting complex. Proc Natl Acad Sci U S A. 2009;106(43):18213–8.
30. Li Z, Wang Y, Li Y, Yin W, Mo L, Qian X, et al. Ube2s stabilizes beta-Catenin through K11-linked polyubiquitination to promote mesendoderm specification and colorectal cancer development. Cell Death Dis. 2018;9(5):456–69.
31. Symons LK, Miller JE, Kay VR, Marks RM, Liblik K, Koti M, et al. The immunopathophysiology of

endometriosis. Trends Mol Med. 2018;24(9):748–62.
32. Chen J, Huang Z, Chen Y, Tian H, Chai P, Shen Y, et al. Lactate and lactylation in cancer. Signal Transduct Target Ther. 2025;10(1):38–64.
33. Chapron C, Marcellin L, Borghese B, Santulli P. Rethinking mechanisms, diagnosis and management of endometriosis. Nat Rev Endocrinol. 2019;15(11):666–82.
34. Maulitz L, Stickeler E, Stickel S, Habel U, Tchaikovski SN, Chechko N. Endometriosis, psychiatric comorbidities and neuroimaging: estimating the odds of an endometriosis brain. Front Neuroendocrinol. 2022;65:100988.
35. Salliss ME, Farland LV, Mahnert ND, Herbst-Kralovetz MM. The role of gut and genital microbiota and the estrobolome in endometriosis, infertility and chronic pelvic pain. Hum Reprod Update. 2021;28(1):92–131.
36. Duan J, Liu X, Wang H, Guo SW. The M2a macrophage subset May be critically involved in the fibrogenesis of endometriosis in mice. Reprod Biomed Online. 2018;37(3):254–68.
37. Wu S, Han L, Zhou M, Li X, Luo L, Wang Z, et al. LncRNA AOC4P recruits TRAF6 to regulate EZH2 ubiquitination and participates in trophoblast Glycolysis and M2 macrophage polarization which is associated with recurrent spontaneous abortion. Int Immunopharmacol. 2023;125(Pt B):111201–15.
38. Sun SM, Zhao BW, Li YY, Liu HY, Xu YH, Yang XM, et al. Loss of UBE2S causes meiosis I arrest with normal spindle assembly checkpoint dynamics in mouse oocytes. Development. 2024;151(6).
39. Bao YY, Zhong JT, Shen LF, Dai LB, Zhou SH, Fan J, et al. Effect of Glut-1 and HIF-1alpha double knockout by CRISPR/CAS9 on radiosensitivity in laryngeal carcinoma via the PI3K/Akt/mTOR pathway. J Cell Mol Med. 2022;26(10):2881–94.
40. Deng Y, Ma J, Zhao S, Yang M, Sun Y, Zhang Q. Expression of glucose transporter-1 in follicular lymphoma affected tumor-infiltrating immunocytes and was related to progression of disease within 24 months. Transl Oncol. 2023;28:101614–24.